JOURNAL OF QUATERNARY SCIENCE (2021) **36**(3) 339–359 ISSN 0267-8179. DOI: 10.1002/jqs.3282

JQS Journal of Quaternary Science QRA Quaternary Research Association

Evidence for centennial-scale Lateglacial and early Holocene climatic complexity from Quoyloo Meadow, Orkney, Scotland

RHYS G. O. TIMMS,[1]* ASHLEY M. ABROOK,[1] IAN P. MATTHEWS,[1] CHRISTOPHER P. FRANCIS,[1] AGNIESZKA MROCZKOWSKA,[2,3] IAN CANDY,[1] STEPHEN J. BROOKS,[4] ALICE M. MILNER[1] and ADRIAN P. PALMER[1]

[1]Centre for Quaternary Research, Department of Geography, Royal Holloway University of London, Surrey, UK
[2]Polish Academy of Sciences, Stanisław Leszczycki Institute of Geography and Spatial Organisation, Warsaw, Poland
[3]University of Lodz, Faculty of Geographical Sciences, Department of Geomorphology and Palaeogeography, Lodz, Poland
[4]Department of Life Sciences, Natural History Museum, London, UK

Received 30 October 2020; Revised 26 January 2021; Accepted 28 January 2021

ABSTRACT: The influence of the North Atlantic on the margins of Europe means the region is particularly sensitive to changes in the ocean–atmospheric system. During the Last Glacial–Interglacial Transition (16–8 cal ka BP) this system was repeatedly disrupted, leading to a series of abrupt and short-lived shifts in climate. Despite much research, the number and magnitude of these 'centennial-scale' events is not well understood. To address this, we expand upon investigations at Quoyloo Meadow, Orkney, Scotland, one of the best chronologically constrained palaeoclimate records in northern Britain. By coupling stable isotope and chironomid fossil analyses with existing data, this study identifies multiple phases of centennial-scale disturbance at: *c.* 14.0, 11.1, 10.8, 10.5, 10.45 and 10.3 cal ka BP, with the events at 14.0 and 10.3 exhibiting a particularly pronounced cold-climate signature. During the Holocene, the strongest response to climate forcing was at *c.* 10.3–10.0 cal ka BP, expressed as a two-stage drop in mean July temperatures, a shift in pollen spectra indicative of 'less-stable' climatic regimes, and a depletion in $\delta^{18}O$ values. We interpret this as the first reliably dated incidence of the '10.3-ka event' in the British Isles and consider the wider impact of this climatic reversal in other Holocene records.

KEYWORDS: abrupt climate change; Chironomidae; Holocene; NW Europe; stable isotopes

Introduction

Abrupt climatic and environmental changes during the Last Glacial–Interglacial Transition (LGIT; 16–8 cal ka BP) are thought to have been driven by reconfigurations of the ocean–atmospheric system (Broecker and Denton, 1990; Clark *et al.*, 2002; Steffensen *et al.*, 2008). This resulted in millennial-scale oscillations that characterized much of the late Pleistocene (Ruddiman *et al.*, 1989; Dansgaard *et al.*, 1993), but also led to a series of shorter-lived centennial-scale events that preferentially impacted the North Atlantic region (Bond *et al.*, 1997). The best resolved records of this period are the Greenland ice cores and these have become the *de facto* regional stratotype for comparison (Björck *et al.*, 1998; Lowe *et al.*, 2008; Rasmussen *et al.*, 2014). However, several climatic oscillations have been detected in European and North American archives which have no comparable analogue within the ice-core records (e.g. Marshall *et al.*, 2002; Whittington *et al.*, 2015), suggesting that some climatic changes are more clearly represented in terrestrial records. Despite a wealth of research into the LGIT, shorter-lived 'centennial-scale' events are not routinely identified and may often be overlooked due to a lack of stratigraphic, proxy sampling and temporal resolution within terrestrial archives. The temporal precision afforded by radiocarbon dating during this period, although excellent, has also probably led to the misallocation and conflation of events in some circumstances (e.g. Baillie, 1991; Lowe and Walker, 2000; Blaauw *et al.*, 2007; Blaauw, 2012). Consequently high-resolution, temporally well-constrained records of climate are needed from across the mid-latitudes to understand the frequency and magnitude of these less 'well-defined' events, and to assess the complexities of climate change during, and immediately following, periods of rapid climatic adjustment.

One such archive that fits this remit is Quoyloo Meadow on Orkney Mainland (Fig. 1). Previous work at the site has established the presence of a sedimentary sequence spanning the LGIT (Bunting, 1994), and recent high-resolution investigations by Abrook *et al.* (2020a) and Timms *et al.* (2017) have detected a number of abrupt changes in the palynological record that are bracketed by cryptotephra of known age. This site can therefore provide detailed information with regard to the number and timing of centennial-scale climatic events during the LGIT. Here we present climatic proxy data in the form of new stable isotope and chironomid-inferred temperature reconstructions for the LGIT with improved chronological and proxy control, particularly for the early Holocene period. The aim of this study is to better constrain and understand the impact of centennial-scale climatic events on the landscape of northern Britain.

Site Context

The Orkney Isles lie 10–90 km north of mainland Scotland and possess a cool maritime climate with a mean annual temperature of 10.7 °C (Met Office, 2020). Their location means they are critically placed to record the glacial and palaeoenvironmental history of northern Britain and the adjacent North Sea basin

*Correspondence: Rhys G. O. Timms, as above.

E-mail: rhys.timms@rhul.ac.uk

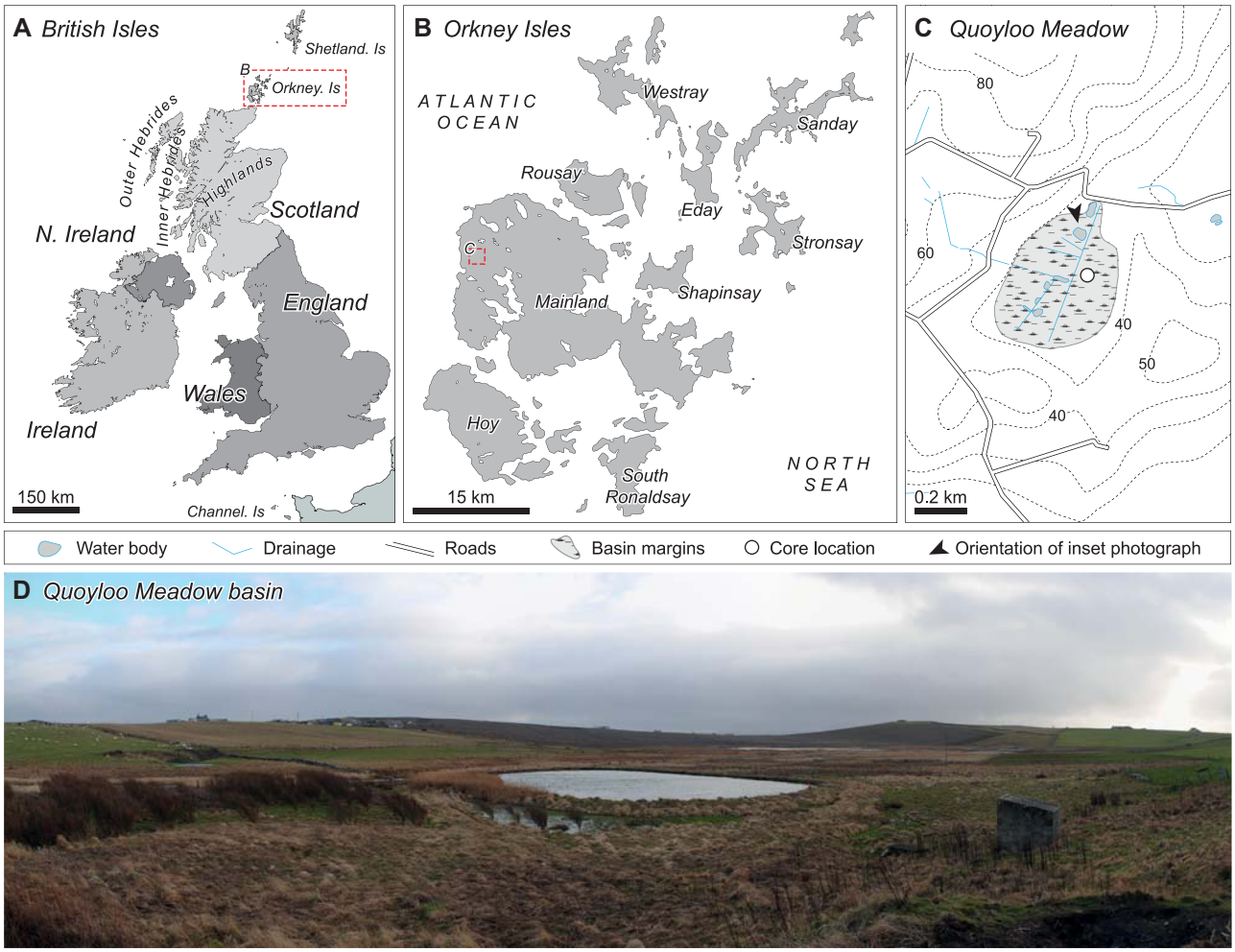

Figure 1. (A) The British Isles and regional context of the Orkney Isles. (B) The Orkney Isles and location of the Quoyloo Meadow site. (C) Local map of the Quoyloo Meadow basin and core site location. Six 50 × 5-cm overlapping Russian cores, in two parallel sequences, were extracted from the eastern margins of the basin following depth sounding on a north-northeast-trending transect. (D) Photograph of the Quoyloo Meadow basin facing south south-east. [Color figure can be viewed at wileyonlinelibrary.com].

(Fig. 1). The Orkney Isles exhibit a complex glacial history (e.g. Rae, 1976, Hall *et al.*, 2016), with cosmogenic dating of glacial erratics and ice-moulded bedrock suggesting final deglaciation from the Devensian ice sheet *c.* 15–17 ka BP (Phillips *et al.*, 2008; Clark *et al.*, 2012). Previous palaeoenvironmental studies have established that the islands experienced a reduced floral diversity compared to the Scottish mainland during the LGIT (Moar, 1969; Bunting, 1994; Whittington *et al.*, 2015; Abrook *et al.*, 2020a), but were later characterized by a rich woodland environment that provided an important resource for Mesolithic and Neolithic communities (Bunting, 1994; Farrell *et al.*, 2014).

Quoyloo Meadow is situated on Orkney Mainland, the largest of the islands in the archipelago (Fig. 1; 59.066417/−3.309333). The basin lies at *c.* 30 m asl within a topographic depression underlain by Devonian Upper and Lower Stromness flagstones (Mykura *et al.*, 1976). At present a valley mire occupies the site, but previous studies have identified a shallow lacustrine sequence with a sedimentary, biostratigraphic and tephrostratigraphic succession typical of the LGIT (Bunting, 1994; Timms *et al.*, 2017; Abrook *et al.*, 2020a).

Methods

Core extraction and sedimentology

The Quoyloo Meadow basin was cored in February 2014 (Timms, 2016). Six 50 × 5-cm overlapping Russian cores were aligned on matching sedimentological units to form the Quoyloo Meadow 1 (QM1) composite sediment stratigraphy with a total depth of 242 cm (Fig. 2). This composite forms the basis of the record reported here, as well as the tephra investigation reported in Timms *et al.* (2017), and the palynological study of Abrook *et al.* (2020a).

The QM1 sequence was described using the Troels-Smith (1955) classification scheme with bulk sedimentological analyses, including loss on ignition (LOI) for organic content, and an estimation of calcium carbonate and magnetic susceptibility performed following methods outlined by Timms *et al.* (2017).

Chronology

Ten cryptotephras and one visible ash layer have been reported from the Quoyloo Meadow sequence (Timms *et al.*, 2017, 2019). Details of those tephra, their stratigraphic placing and current best age estimates are given in Table 1. This tephrochronological information has been used to generate an age–depth model in OxCal V4.4.2 utilizing the IntCal20 calibration curve (Bronk Ramsey, 2017; Reimer *et al.*, 2020). Model outputs were computed using a '*P_Sequence*' depositional model (Bronk Ramsey, 2008) and utilized a variable 'k' parameter which enabled the computation to determine an optimized age–depth relationship (Bronk Ramsey and Lee, 2013).

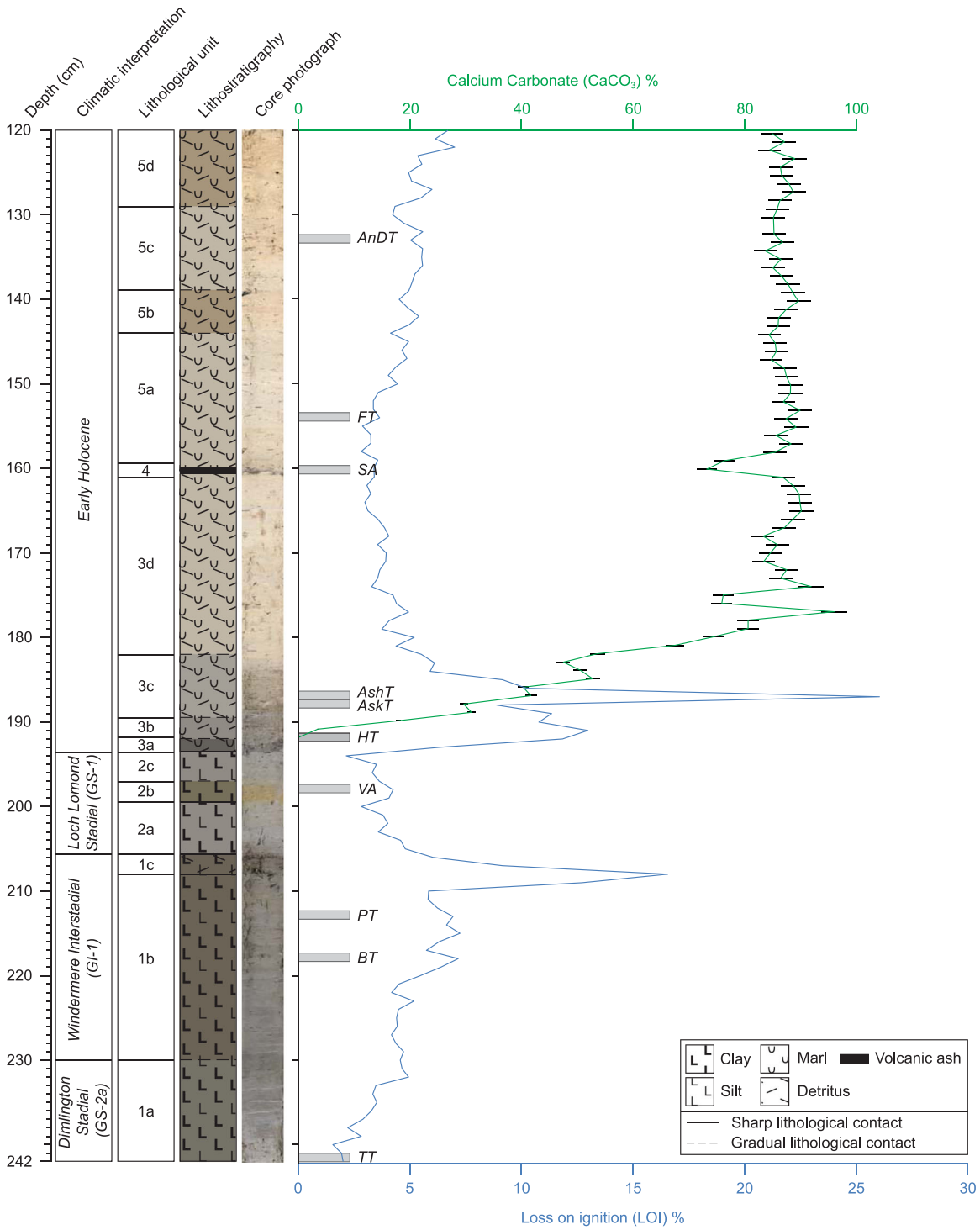

Figure 2. The QM1 composite sediment stratigraphy from Quoyloo Meadow. Loss on ignition (LOI) and calcium carbonate ($CaCO_3$) content are also shown. The grey horizontal bars mark the primary position of nine cryptotephra and one visible tephra reported in Timms *et al.* (2017, 2019). The abbreviations of the tephra are as follows: TT, Tanera Tephra; BT, Borrobol Tephra; PT, Penifiler Tephra; VA, Vedde Ash; HT, Hässeldalen Tephra; AskT, Askja-S Tephra; AshT, Ashik Tephra; SA, Saksunarvatn Ash; FT, Fosen Tephra; and AnDT, An Druim Tephra. A detailed lithological description is given in Supporting Information Table S2. [Color figure can be viewed at wileyonlinelibrary.com].

Chironomids

In total, 35 samples were analysed for chironomid head capsule content. The sampling occurred in two stages with an outline low-resolution scan, and an increased sampling resolution at intervals where temperature fluctuations were initially detected. Extraction of head capsules followed standard procedures described in Brooks *et al.* (2007). Sediment subsamples of 0.25–3.94 g were gently heated in 10% sodium hydroxide (KOH) at 75 °C for 10–15 min. Residual material was passed through 120- and 90-μm sieves under running water, with both size fractions examined for head capsule content at 100× to 400× magnifications. Extracted head capsules were mounted onto glass slides using Euparal, and species identification followed reference guides: Wiederholm (1983), Moller Pillot and Klink (2003) and Brooks *et al.* (2007).

Two calibration datasets, the Norwegian and the combined Swiss–Norwegian, were tested for the chironomid-inferred mean July air temperature (C-IT; T_{Jul}) reconstruction at Quoyloo Meadow (Brooks and Birks, 2001; Heiri *et al.*, 2011). The combined Swiss–Norwegian calibration dataset was

Table 1. Age estimates for tephra identified within the QM1 sequence (see Timms *et al.*, 2017, 2019). These tephra form the basis of the Bayesian age-model presented in Fig. 3. Tephra age estimates have been recalculated using the cross-referenced Bayesian age-model presented in Kearney *et al.* (2018) and updated with the IntCal20 calibration curve (Reimer *et al.*, 2020). The age estimate for the An Druim Tephra is derived from a Bayesian age-model of the Lochan An Druim type-site (see Ranner *et al.*, 2005; Timms, 2016) and updated with the IntCal20 calibration curve (Reimer *et al.*, 2020). The input age of the Fosen Tephra is derived from Lind *et al.* (2013) and given an arbitrary 1σ error range of 100 years due to the absence of a reported age uncertainty (see Timms *et al.*, 2017). The age estimates for the Borrobol and Penifiler tephras were inputted into the model as 'priors' due to their non-normal distribution; hence they are presented here as ranges only. The age estimate of the Tanera Tephra was not used in the construction of the age-model but is instead the result of age-model extrapolation to the base of the QM1 sequence. Ages marked with an asterisk denote the most reliable age estimates for these tephra at present

Tephra	Depth (cm)	Input age estimate ($\mu \pm 1\sigma$) (cal a BP)	Input age range (95.4% confidence interval) (cal a BP)	Output age estimate ($\mu \pm 1\sigma$) (cal a BP)	Output age range (95.4% confidence interval) (cal a BP)
An Druim Tephra	133	9652 ± 86	9480–9824	9670 ± 70*	9528–9812*
Fosen Tephra	154	10 200 ± 100	10 000–10 400	10 125 ± 76*	9961–10 262*
Saksunarvatn Ash	160	10 177 ± 49*	10 079–10 275*	10 190 ± 46	10 099–10 280
Askja-S Tephra	188	10 811 ± 50*	10 711–10 911*	10 823 ± 51	10 720–10 925
Hässeldalen Tephra	193	11 301 ± 67*	11 167–11 435*	11 204 ± 159	10 827–11 428
Vedde Ash	198	11 997 ± 35*	11 927–12 067*	11 996 ± 36	11 924–10 067
Penifiler Tephra	213	–	13 830–14 120*	–	13 843–14 127
Borrobol Tephra	218	–	14 040–14 310*	–	14 034–14 282
Tanera Tephra	242	–		15 300 ± 899*	14 123–17 130*

selected over the Norwegian for several reasons. First, the incorporation of carbonate lakes from the Swiss calibration dataset means the combined dataset contains records with similar lake chemistry to Quoyloo Meadow during the Holocene. Second, the combined calibration dataset contains a greater number of chironomid taxa/morphotypes and those that are 'rare' in the Norwegian calibration dataset are present in greater abundance. Third, the combined calibration dataset has superior validation statistics compared to the Norwegian dataset (see Supporting Information Table S1).

The selected Swiss–Norwegian combined calibration dataset consists of 274 lakes spanning a temperature gradient of 3.5–18.4 °C (Heiri *et al.*, 2011). Nineteen outlier lakes were deleted from the calibration as defined by Heiri *et al.* (2011). A two-component, weighted averaging-partial least squares (WA-PLS) regression model was used on square-root-transformed fossil data, which gave a root mean squared error of prediction (RMSEP) of 1.4 °C, a coefficient of determination (r^2_{boot}) of 0.9 and a maximum $bias_{boot}$ of 0.8 °C. Sample-specific errors were calculated using 999 bootstrapping cycles.

Five criteria were used to assess the reliability of the C-IT reconstruction:

(i) A goodness-of-fit to temperature was assessed by passively plotting fossil samples within a canonical correlation analysis (CCA) of the modern calibration dataset. Fossil samples which had a squared residual distance value exceeding the 90th and 95th percentiles of samples in the modern calibration dataset had a 'poor' or 'very poor' fit to temperature, respectively (Telford, 2014a). CCA was conducted on untransformed data in R using the vegan package (Oksanen *et al.*, 2017).
(ii) The modern analogue technique (MAT) was employed to assess if fossil samples had good analogues in the modern calibration dataset, with chi-squared used as a measure of dissimilarity. Samples with distances to the closest analogue larger than the 5th and 10th percentile of all modern distances were treated as having 'no close' and 'no good' analogue, respectively (Telford, 2014b). MAT analysis was performed on untransformed data using the analogue package in R (Simpson, 2020).
(iii) No more than 5% of fossil assemblages should be from taxa that are rare in the modern calibration dataset – defined as having a Hill's N2 value of less than 5 (Heiri *et al.*, 2003).
(iv) In total, 95% of taxa in fossil samples should be present in the modern calibration dataset (Birks, 1998).
(v) Samples with a minimum of 45–50 head-capsules are considered reliable (Heiri and Lotter, 2001).

Where these criteria are not met, however, samples are retained but are considered with further caution.

Stable isotopes ($\delta^{18}O$ and $\delta^{13}C$)

Sediment subsamples of *c.* 0.5 cm^3 were sampled contiguously at 0.5-cm resolution from the marl substrate between 195 and 150 cm. Subsamples were disaggregated with 0.5% sodium hexametaphosphate $(NaPO_3)_6$, before sieving at 63 μm to remove detrital material and biogenic carbonate contamination, e.g. molluscs and ostracods. Sieved samples were air dried and treated with 10% hydrogen peroxide (H_2O_2) to remove organic material. Samples were homogenized and weighed to a mass of 500–1100 μg, but samples exhibiting <10% $CaCO_3$ were weighed to *c.* 1500 μg. $\delta^{18}O$ and $\delta^{13}C$ values were determined by analysing the CO_2 evolved from a reaction of the sample with phosphoric acid (H_3PO_4) at 90 °C using a VG PRISM series 2 mass spectrometer. Internal (RHBNC) and external (NBS19, LSVEC) standards were run to check for machine precision and drift. All stable isotopic values are quoted with reference to VPDB.

Palynology, charcoal and principal curve analysis

The methodologies for pollen, charcoal and principal curve (PrC) analyses are outlined in Abrook *et al.* (2020a), where further detail on these data series can be accessed. PrC analysis is a non-parametric statistical method that is particularly sensitive in the identification of gradients in ecological data. PrC analysis, which starts with principal components analysis (PCA) or CA axis 1 scores as the starting curve, is defined as a smooth one-dimensional curve passing through an *m*-dimensional dataspace (Hastie and Stuetzle, 1989; De'ath, 1999; Simpson and Birks, 2012). To generate the PrC, the starting curve is iterated, using smoothing splines resulting in increased fit to the data. This method was selected as PrCs capture more variance within datasets than standard ordination techniques (Simpson and Birks, 2012).

Results

Sedimentology

The composite sediment stratigraphy, bulk sedimentological indicators and tephrostratigraphy from Timms *et al.* (2017, 2019) is presented in Fig. 2 with a summary outlined below. More detailed sedimentological information is provided in Supporting Information Table S2.

A dark grey silty-clay unit, with low organic content (*c.* 2–7%) is present at the base of the QM1 sequence (Unit 1a/1b). Organic content increases in Unit 1c with the occurrence of highly humified organic detritus (*c.* 17%). These organic sediments return to lower values (*c.* 4%) as the sequence transitions into the overlying minerogenic unit. Units 2a to 2c are characterized by a light grey silty-clay (organic content *c.* 2–5%), with Unit 2b possessing an orange/brown coloration, a feature probably caused by the leaching and dissolution of basaltic glass shards (Timms *et al.*, 2017). Units 3a–3d are characterized by the precipitation of a buff-coloured marl substrate, signalling a significant shift in environmental conditions. Organic values initially peak in Units 3a–3b (*c.* 11–13%), but begin to fall in Units 3c–3d as carbonate sedimentation becomes more dominant in the basin ($CaCO_3$ values *c.* 40–90%). At 160 cm a black horizontal band approximately 0.5 cm thick of fine-grained volcanic ash intersects the marl substrate ($CaCO_3$ values *c.* 70%). Above this, marl sedimentation resumes ($CaCO_3$ values 80–90%) and continues to the top of the studied sequence (Units 5a–5d).

Chronology

The age model derived from the tephrostratigraphic findings of Timms *et al.* (2017, 2019), and updated to include the tephra's current best age estimates (Table 1), exhibits good agreement indices and suggests that the onset of sedimentation in the Quoyloo Meadow basin began at *c.* 15.30 ± 1.80 cal ka BP (Fig. 3). Age estimates are reported at 2σ uncertainty unless otherwise stated.

Chironomids

A total of 53 different chironomid morphotypes were identified. Using the CONISS method (Grimm, 1987), five chironomid assemblage zones were identified (Fig. 4): QMC-1 (242–206 cm), QMC-2 (206–190 cm), QMC-3 (190–162 cm), QMC-4 (162–147 cm) and QMC-5 (147–121 cm). The chironomid dataset is presented in full in Supporting Information Table S1.

QMC-1 is largely composed of cool-temperate and temperate indicating taxa including *Psectrocladius sordidellus*-type (17%), *Microtendipes pedellus*-type (16%) and *Chironomous anthracinus*-type (10%), with smaller but still significant contributions from *Dicrotendipes* (5%) and *Thienemannimyia* (3%). Taxa with cold and ultra-cold optima are present in very low numbers, but at 214 cm *Micropsectra insignalobus*-type and *Micropsectra radialis*-type peak temporarily at 12% and 10%, respectively.

A change occurs in QMC-2 with cold and ultra-cold indicating taxa including *M. radialis*-type (31%) and *M. insignilobus*-type (21%) dominating. Other taxa with cold temperature optima that are consistently present in abundance are *Pseudodiamesa* (6%), *Paratanytarsus austriacus*-type (5%) and *Paracladius* (4%). Cool-temperate, temperate and warm indicating taxa reduce to very small abundances or disappear completely.

In QMC-3/4/5 the chironomid assemblage is composed of cool-temperate, temperate and warm indicating chironomids. *Tanytarsus glabrescens*-type (32%) is by far the most dominant taxon in each of these zones. Other major contributors include *Thienemannimyia* (8%), *Parakiefferiella* Type A (5%), *Procladius* (5%) and *Ablabesmyia* (4%). However, in QMC-4, some cold and ultra-cold indicating taxa momentarily re-appear including *M. insignilobus*-type, *M. radialis*-type and *Paracladius* with peak values of 36%, 10% and 6% respectively.

Stable isotopes ($\delta^{18}O$ and $\delta^{13}C$)

The $\delta^{18}O$ and $\delta^{13}C$ values obtained from the QM1 sequence exhibit a notable degree of variability between samples (Fig. 5). To highlight trends in the data series, a three-point moving average has been applied. Discussion will be based on these moving averages with the acknowledgement that this may limit some interpretations.

The oxygen isotope record is characterized by a general increase in values from −4.16‰ (194.25 cm) to −3.29‰ (150.25 cm). At several intervals, however, this rising trend is punctuated by short-term decreases in values, labelled as QMO-e1 to e4 (Fig. 5). QMO-e1 is a subtle depletion in isotopic values with a minimum of −4.18‰ centred on 191.25 cm and is bounded by values of −4.11 (193.25 cm) and −3.90‰ (188.75 cm). QMO-e2 exhibits depleted isotopic values of −4.14‰ at 186.25 cm, and is bounded by values of −3.90‰ (188.75 cm) and −3.88‰ (183.75 cm). QMO-e3 reaches a minimum of −3.51‰ at 170.75 cm and is bounded by values of −3.14‰ (173.25 cm) and −3.05‰ (167.25 cm). QMO-e4 is the depletion of greatest magnitude recorded in the QM1 sequence, with values of −2.93‰ (159.25 cm) falling to −3.44‰ at 156.75 cm before recovering to −3.03‰ (154.75 cm).

The carbon isotope record exhibits an opposing trend: enriched values typify the base of the carbonate sequence, falling from 3.07‰ at 194.25 cm to 1.20‰ at 150.25.

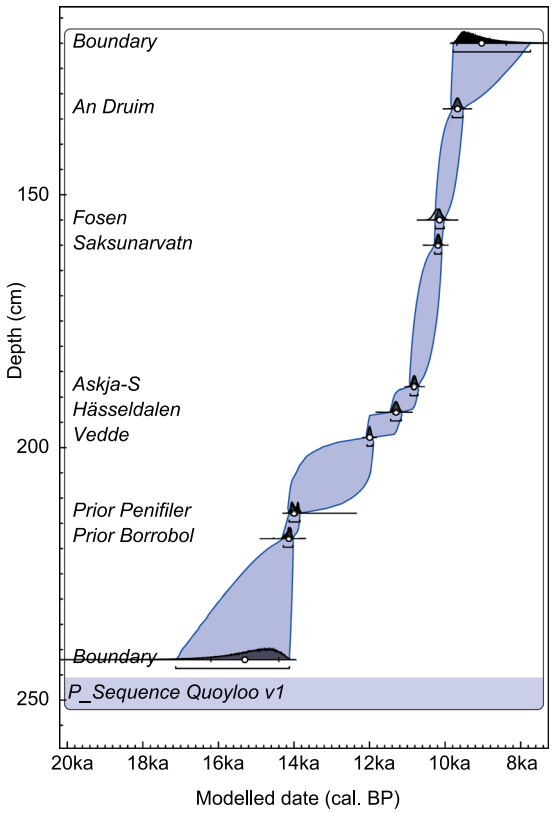

Figure 3. The age–depth (*P_Sequence*) depositional model for Quoyloo Meadow based on the tephrostratigraphic findings of Timms *et al.* (2017, 2019), and updated from Abrook *et al.* (2020a) to include the current best age-estimates for the tephra (Table 1). Age uncertainties are plotted as 95.4% confidence intervals. [Color figure can be viewed at wileyonlinelibrary.com].

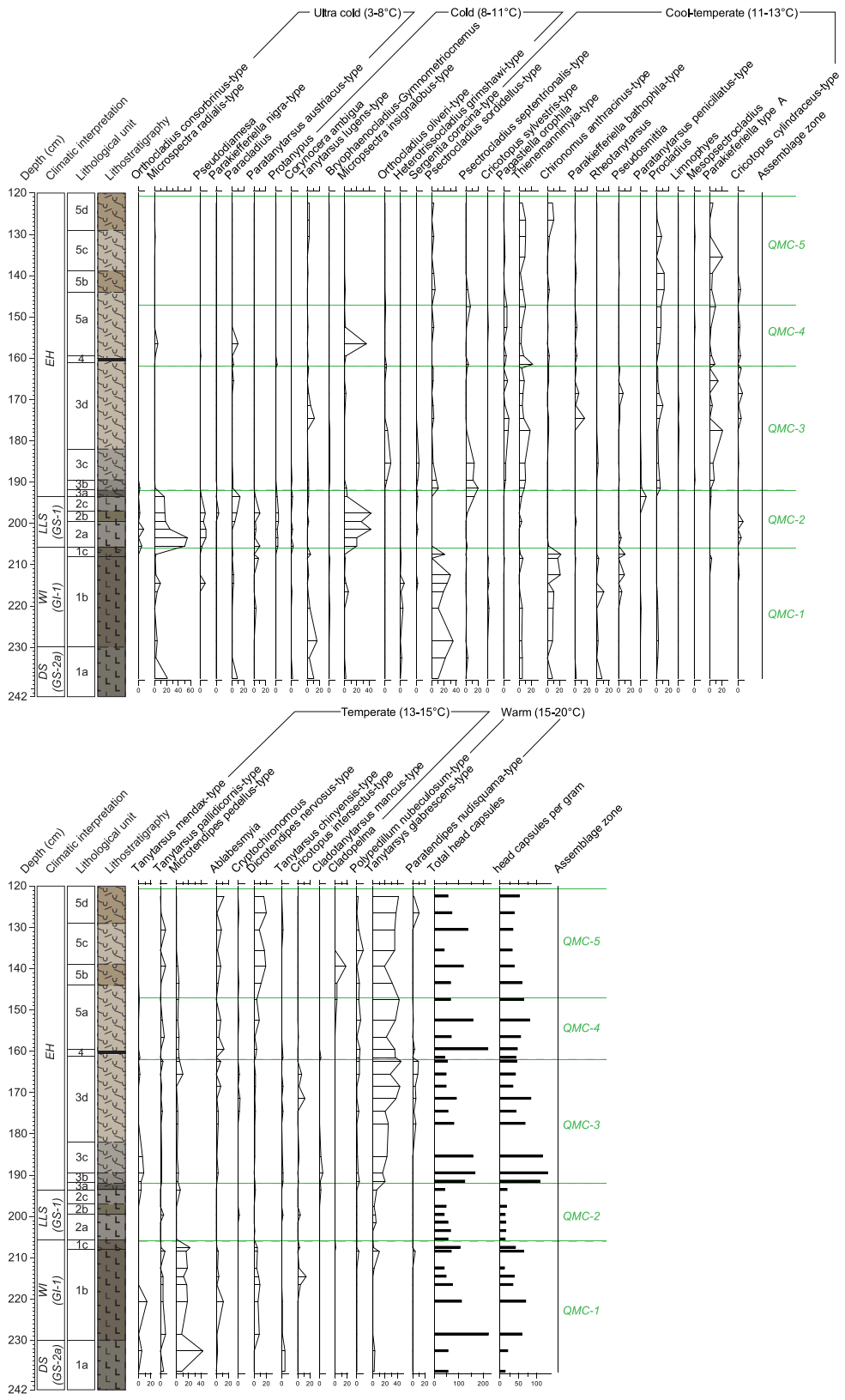

Figure 4. Percentage abundance diagram of the main chironomid taxa present at Quoyloo Meadow. Chironomid assemblage zones are noted as QMC-1 to -5. Taxa are arranged by their temperature optima in the modern calibration dataset (Heiri *et al.*, 2011) as calculated using a weighted-averaging model. Head-capsules per gram and total head-capsule counts are also displayed. For lithological information refer to Fig. 2. [Color figure can be viewed at wileyonlinelibrary.com].

Pollen and PrC

The pollen profile at Quoyloo Meadow is divided into 11 local pollen assemblage zones based on variations in principal taxa (Fig. 6; Abrook *et al.*, 2020a). The PrC has open herbaceous vegetation and *Corylus*/*Betula* woodland as its two end members (at the base and top of the sequence respectively). As 81% of the variation in the palynological dataset can be explained by the PrC, fluctuations in the curve throughout the sequence probably relates to compositional change in the vegetation on the landscape (Fig. 6; Abrook *et al.*, 2020a).

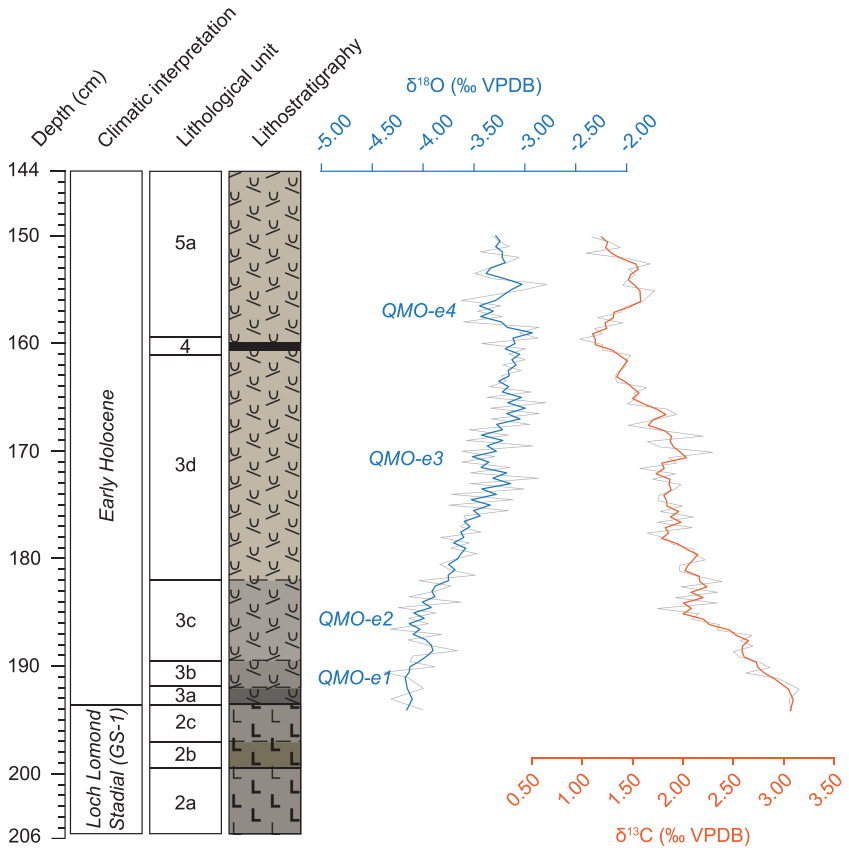

Figure 5 ^{18}O and ^{13}C fluctuations recorded in the early Holocene sequence at Quoyloo Meadow. Original data are shown in grey with the overlying coloured line representing a three-point moving average (see main text for details). Episodes of depletion or isotopic 'events' are labelled as QMO-e1 to -e4, and are centred on the following depths: QMO-e1 (191.25 cm); QMO-e2 (186.25 cm); QMO-e3 (170.75 cm); QMO-e4 (156.75 cm). All values are shown as variations in relation to VPDB. For analytical uncertainties associated with the measurements refer to Supporting Information Table S3. For lithological information refer to Fig. 2. [Color figure can be viewed at wileyonlinelibrary.com]

QMP-1 (223-217 cm) and QMP-2 (217-201 cm) are dominated by herbaceous pollen with dominant taxa including Poaceae and *Rumex*. Within these two zones *Betula* percentages increase throughout. At 212.5 and 211.5 cm a small inflection in the PrC is noted, which appears to be driven by reductions in *Betula* and increases in *Rumex*. Throughout these zones percentages for the non-pollen palynomorph *Pediastrum* are high (37%).

QMP-3 (210–202 cm) exhibits high percentages of *Empetrum nigrum* which occurs alongside *Pediastrum* and later increases in *Artemisia*. QMP-4 (202–192 cm) is predominantly composed of *Artemisia* and *Pediastrum* albeit with generally lower percentages than previous zones. Additional taxa throughout the upper levels of QMP-3 and QMP-4 include Poaceae, Cyperaceae, Saxifragaceae and *Selaginella selaginoides*. Within QMP-3 and QMP-4 the largest shift in the PrC can be observed, signalling a considerable change to vegetation type and cover (Fig. 6).

QMP-5 (192–189 cm) and QMP-6 (189–184 cm) exhibit successive peaks of *Pediastrum*, *Empetrum nigrum* and *Betula*. Between QMP-7 and QMP-10 (164–136 cm) there is a general trend towards lower *Betula* percentages but an increase in herbaceous pollen types. *Corylus* increases from QMP-7 and is dominant by QMP-11 (136–131 cm) alongside *Betula*. At two additional locations between QMP-5 and QMP-11 a plateau in the general shift towards lower values or short inflections in the PrC were noted by Abrook *et al.* (2020a). These occur from 188.5 to 185.5 cm and 158.5 to 154.5 cm and appear to be driven by variability in *Empetrum nigrum*, *Betula* and Poaceae.

Charcoal

Multiple phases of increased charcoal abundance are identified throughout the profile with charcoal numbers ranging from 1 to 62 fragments cm^{-3} (Fig. 6; Abrook *et al.*, 2020a). The most prominent of these phases are identified at 222.5–221.5, 203.5, 197.5, 180–189.5, 154 and 147–144.5 cm. Greater charcoal accumulations appear within the marl sediments in association with zones QMP-6 to QMP-9. Further increased concentrations appear to coincide with changes in vegetation as indicated by the PrC (Abrook *et al.*, 2020a).

Palaeoenvironmental significance of the proxy record (chironomids)

Of the 36 chironomid samples analysed, 20 have a good fit-to-temperature while four have a poor fit and 12 have a very poor fit. The majority of samples with a poor or very poor fit-to-temperature occur in the early Holocene (QMC-3 and QMC-5; Fig. 7) and are possibly caused by the high abundance of *Tanytarsus glabrescens*-type (up to 47%) which is present only in 16 lakes of the calibration dataset. The exceptions to this are sections of QMC-4 and -5 between 160–150 and 145–140 cm where a good fit to temperature is seen. The majority of samples in QMC-1 and QMC-2 (LLS and WI; Fig. 7) have good analogues, in contrast to samples in QMC-3, -4 and -5 which have poor or very poor analogues in the modern calibration data. This suggests the Holocene lake established at Quoyloo Meadow was relatively unlike the lakes contained within the calibration dataset. However, WA-PLS inference models have been shown to perform surprisingly well in non-analogous situations (Birks *et al.*, 2010; Brooks *et al.*, 2012).

All samples have at least the recommended minimum of 45–50 head-capsules except for 212.5, 199.5 and 135.5 cm which have 43, 43 and 41 head-capsules respectively. Despite the low number of head capsules in these particular samples, the taxa are very similar to neighbouring intervals. This suggests that species composition and thus ecological and temperature inferences are not excessively limited or biased by the low recovery rate. A single head-capsule was found at 241.5 cm (*Micropsectra radialis*-type) and has been excluded from all numerical analysis. The only taxon not present in the modern dataset is *Parakiefferiella* Type-Swiss (Brooks and Heiri, 2013) which is present in only four samples and forms

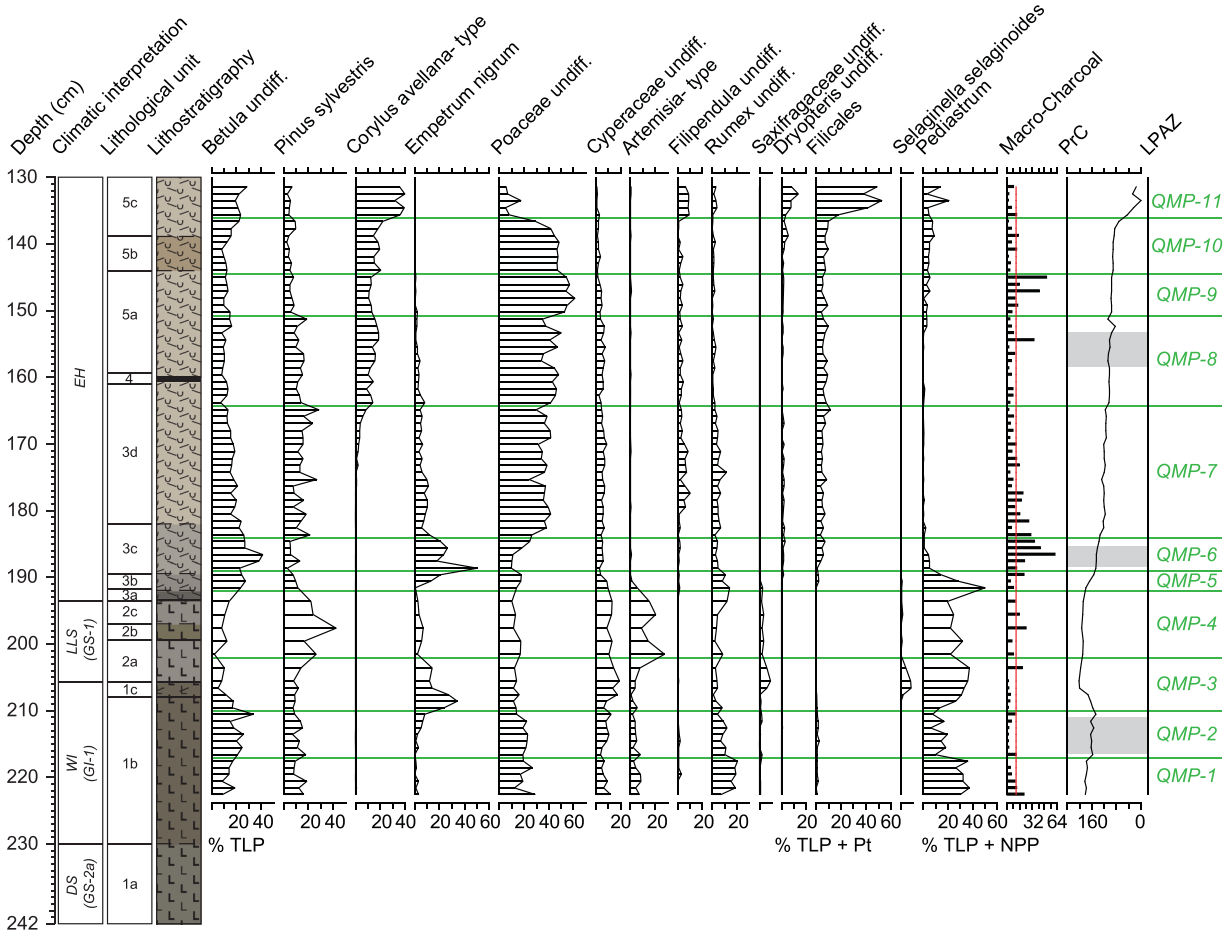

Figure 6. Selected pollen, pteridophyte and non-pollen palynomorphs (NPP) from Quoyloo Meadow. Key taxa are shown with the addition of local pollen assemblage zones (LPAZ) and a principal curve (PrC) with key phases of variability shown in grey (see text for explanation). Macro-charcoal counts are included with areas higher than the average (red) deemed important. All data are presented as percentages of total land pollen (TLP) unless stated (see Abrook *et al.*, 2020a). For lithological information refer to Fig. 2. [Color figure can be viewed at wileyonlinelibrary.com].

less than 4.2% of individual sample assemblages. Taxa which are rare in the modern dataset and present in the record include *Tanytarsus nemorosus*-type, *Tanytarsus lactescens*-type, *Parakiefferiella nigra*-type, *Nilotanypus* and *Diamesa aberrata*-type. These are only present in six samples and comprise no more than 4% of fossil samples. Therefore, these should not significantly affect the temperature reconstruction.

Present in the C-IT reconstruction are a series of short-lived oscillations labelled QMC-e1-e3 (Fig. 7). T_{Jul} values throughout QMC-1 are *c.* 12 °C, with a decline noted at 214.5 cm (QMC-e1). In QMC-2, T_{Jul} is *c.* 7 °C, notably lower than the previous zone. A large rise in T_{Jul} is present at the end of QMC-2 with values continuing to rise throughout QMC-3, albeit with a slight inflection at 174.5 cm (QMC-e2). A decline of *c.* 3.8 °C is observed in QMC-4 (QMC-e3), with T_{Jul} reaching a minimum of 14.2 °C. T_{Jul} recovers in QMC-5 and reaches highs of 16.8 °C. Sample-specific errors range from 1.4 to 1.7 °C.

Palaeoenvironmental significance of the proxy record (stable isotopes)

The $\delta^{18}O$ value of lake carbonates is controlled by two factors: (i) the temperature at which carbonate mineralization occurs and (ii) the $\delta^{18}O$ value of the lake water (Leng and Marshall, 2004; von Grafenstein *et al.*, 2013). In mid-latitude temperate climate regions, such as NW Europe, the modification of the isotopic value of lake waters by processes such as evaporation is minimal (for discussion see Candy *et al.*, 2016). Consequently, in such areas, the $\delta^{18}O$ value of lake water is strongly linked to the $\delta^{18}O$ value of precipitation which is, in turn, heavily dependent upon air temperature (Rozanski *et al.*, 1992). In such a system both of the main influences on lake carbonate $\delta^{18}O$ values are therefore temperature driven, although they work to drive the carbonate isotope values in different directions (Candy *et al.*, 2011). The relationship between oxygen isotope fraction during carbonate mineralization and temperature is well known and is around +0.24‰/−1°C (Leng and Marshall, 2004) effectively meaning that the $\delta^{18}O$ of a carbonate becomes higher under lower temperatures. The relationship between the $\delta^{18}O$ of precipitation and air temperature is, for the mid-latitudes, around +0.58‰/+1°C, resulting in rainfall and surface waters having higher $\delta^{18}O$ values under higher temperatures.

As the magnitude of the air temperature/$\delta^{18}O$ of precipitation relationship is greater than the magnitude of the mineral fractionation/temperature relationship, the $\delta^{18}O$ value of lake carbonates in Europe frequently shows a linear relationship with temperature, i.e. the isotope values decrease as temperatures decline and increase as temperatures rise. This can be seen empirically in LGIT studies on NW European lakes which show $\delta^{18}O$ values decreasing during well-established cold events such as the Loch Lomond Stadial (Marshall *et al.*, 2002), or with cold events observable in independently reconstructed temperature records (Blockley *et al.*, 2018; Abrook *et al.*, 2020b). Such a relationship is also observable in the early Holocene record of Quoyloo Meadow, which shows a long-term trend of increasing $\delta^{18}O$ values associated with increasing T_{Jul} estimates and short-lived declines in $\delta^{18}O$

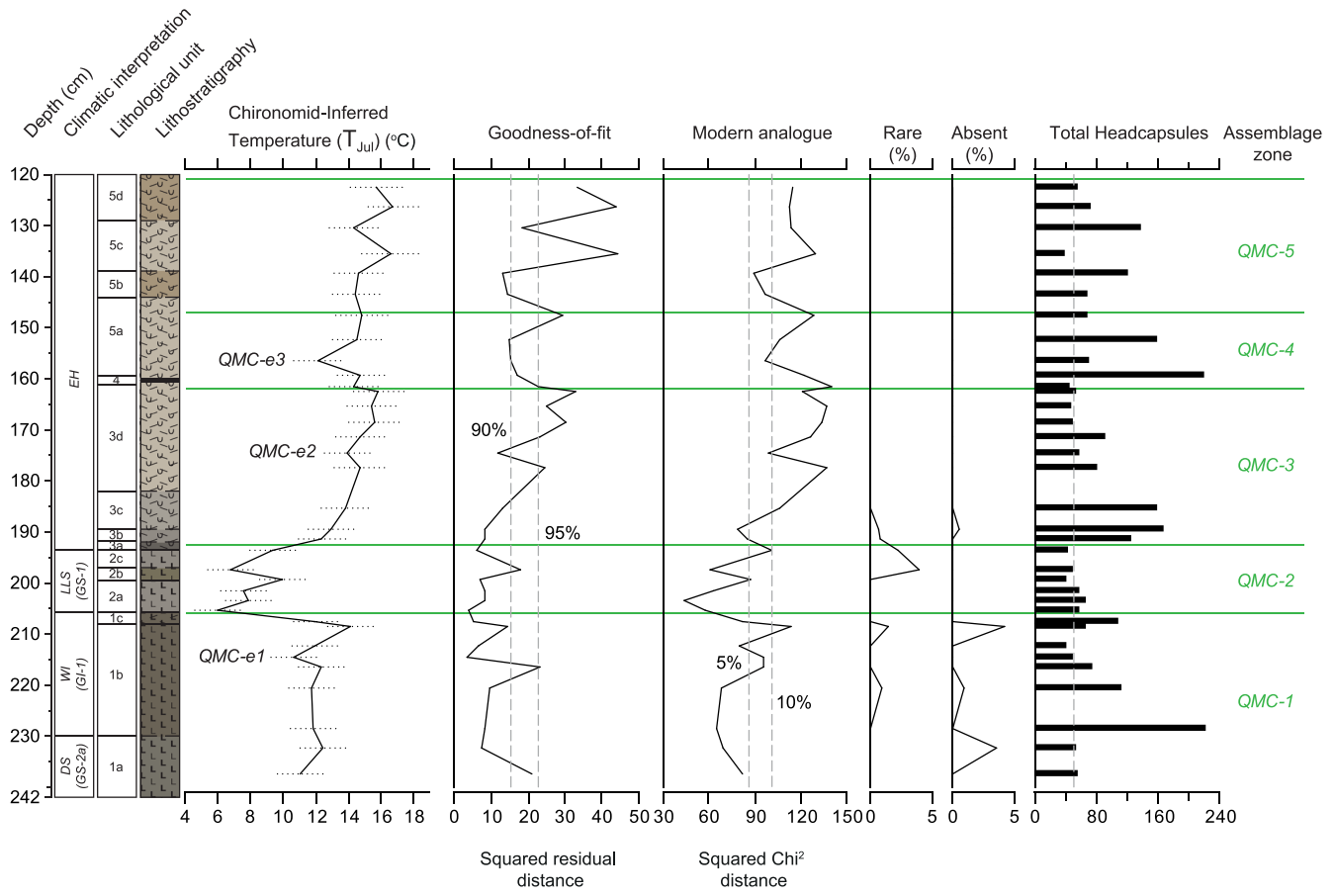

Figure 7. (A) Chironomid-inferred temperature estimates (T_{Jul}) with sample-specific error bars. (B) Nearest modern analogue statistics with dashed lines showing the 5th and 10th percentile of the Chi^2 distances of all samples in the modern calibration dataset. (C) Goodness-of-fit of the fossil assemblages to temperature, with dashed lines representing the 90th and 95th percentiles of squared residual distance of modern samples to the first axis of a CCA. (D) The number of taxa present in the downcore record which are rare in the modern calibration dataset, defined by Hill's N2 < 5. (E) Taxa not present in the modern calibration dataset. (F) Number of head-capsules; samples to the right of the dotted line have more than 50 head-capsules. Short-lived 'centennial-scale' cold climatic episodes or 'events' are labelled as QMC-e1-e3 and are centred on the following depths: QMC-e1 (214.5 cm); QMC-e2 (174.5 cm); QMC-e3 (156.5 cm). For lithological information refer to Fig. 2. [Color figure can be viewed at wileyonlinelibrary.com].

values associated with abrupt decreases in T_{Jul} estimates. It is therefore probable that air temperature changes are the primary control on the $\delta^{18}O$ value of Quoyloo Meadow lacustrine carbonates. Consequently, the $\delta^{18}O$ record of the early Holocene at Quoyloo Meadow is interpreted as recording a long-term trend of climate warming, punctuated by a series of short-lived cooling events.

Such an interpretation assumes that the $\delta^{18}O$ values of lake waters have undergone no major isotopic modification, i.e. through evaporation, during residence within the basin whilst it also assumes that minimal contamination of the isotopic signature by the presence of detrital carbonates (Candy *et al.*, 2015, 2016). Both of these factors are considered unlikely to have been significant in the Quoyloo Meadow record. Evaporation of lake waters has a tendency to produce positive co-variance in both $\delta^{18}O$ and $\delta^{13}C$ values (Talbot, 1990), with greater evaporation producing higher values in both isotope systems, whereas in the Quoyloo Meadow record $\delta^{18}O$ and $\delta^{13}C$ values trend in opposite directions ($\delta^{18}O$ increase whilst $\delta^{13}C$ decrease). Equally, short-term declines in $\delta^{18}O$ values are not matched by corresponding changes in $\delta^{13}C$ values.

It is also considered unlikely that detrital contamination has had an influence on the isotopic record seen in Quoyloo Meadow. The incorporation of limestone bedrock, which has much higher $\delta^{18}O$ and $\delta^{13}C$ values than lacustrine carbonates, into lake sediments can contaminate the isotopic signal, generating particularly high isotopic values (Candy *et al.*, 2015). Whilst dolomitic siltstones and tills with limestone components occur across Orkney (Mykura *et al.*, 1976; Rae, 1976; Hall *et al.*, 2016) it is considered unlikely that these have had an influence on isotopic values. During periods of high detrital inwash, i.e. the Loch Lomond Stadial, carbonate values are 0%, indicating that the surrounding catchment yielded no detrital carbonate during phases of relative landscape instability (see Candy *et al.*, 2016). Furthermore, analyses on samples with low percentage carbonate values, which would, if impacted by detrital contamination, be the most sensitive to limestone inwash and have the highest $\delta^{18}O$ values, yield the lowest $\delta^{18}O$ values of the entire record.

It is worth noting two further features of the Quoyloo Meadow $\delta^{18}O$ record. First, there is a relatively high degree of scatter within the $\delta^{18}O$ dataset. Whilst a three-point moving average produces a stable and clear signal, there is significant variability between stratigraphically contiguous samples. It is likely that this is a function of the high resolution of the record (Mangili *et al.*, 2010; Tye *et al.*, 2016). The chronology for the early Holocene indicates a sedimentation rate of approximately 1 cm per 30 years, whilst the sampling resolution, 0.5 cm per sample, implies that each isotope sample reflects c. 15 years of marl accumulation. In such a record, inter-year and inter-decadal variability in weather and climate will still have an influence on the isotopic values of individual samples and, consequently, a high degree of isotopic variability is to be expected between samples (see Tye *et al.*, 2016). This is true for any isotope dataset constructed through an exceptionally high-resolution lake record. Second, the isotopic record from Quoyloo Meadow

only extends back in time as far as carbonate precipitation occurred within the lake basin. Based on the site chronology this is 11.48 ± 0.48 cal a BP, which means that the Quoyloo Meadow $\delta^{18}O$ record may not span the rapid increase in $\delta^{18}O$ values seen in NGRIP from *c.* 12 to 11.7 ka and, consequently, may not provide a complete record of the very early Holocene. The Quoyloo Meadow $\delta^{18}O$ record does provide a high-resolution snapshot of a small part of the postglacial warming, but it is difficult to establish whether the well-defined isotopic trends seen in NGRIP directly after GS-1 are also expressed in the Quoyloo Meadow record.

Less attention has been paid to the $\delta^{13}C$ values of lacustrine sequences in the British Late Quaternary as they typically reflect changing intra-basin processes rather than wider palaeoclimatic trends (Candy *et al.*, 2016; Blockley *et al.*, 2018). In general, the $\delta^{13}C$ of lacustrine carbonate represents the dissolved inorganic carbon (DIC) pool of the lake system (Leng and Marshall, 2004). The increasingly negative trend seen in the QM1 sequence is common to a number of early Holocene lacustrine records and has been used to indicate the increasing amount of plant-respired carbon dioxide being supplied to the basin as the landscape revegetates after the Loch Lomond Stadial (Blockley *et al.*, 2018). This interpretation is consistent with the pollen data from this site and is proposed to explain the trend that is seen at Quoyloo Meadow.

Interpretation

Palaeoenvironmental changes during the Dimlington Stadial and Windermere Interstadial

The onset of sedimentation at Quoyloo Meadow appears to have begun during the latter phases of the Dimlington Stadial, an interval characterized by glacial retreat and broadly comparable to the GS-2.1a cold phase (Rose, 1985; Walker and Lowe, 2019). This (chrono-)stratigraphic correlation is proposed via three lines of evidence: (i) the dominance of sterile minerogenic sediments within the lowermost units at Quoyloo Meadow (Fig. 2); (ii) the occurrence of the 'Tanera Tephra' (242 cm; 15.30 ± 1.80 cal ka BP), a cryptotephra found within Dimlington Stadial deposits elsewhere in the British Isles (Timms *et al.*, 2019); and (iii) a single chironomid head capsule of *Microspectra radialis-type*, an ultra-cold climate indicator which was identified at 241.5 cm (15.23 ± 1.77 cal ka BP). Together this evidence is suggestive of a cold climate and barren landscape, with sediments accumulating relatively soon after deglaciation.

The first viable chironomid sample occurs at 237.5 cm (15.08 ± 1.58 cal ka BP) and provides an estimated mean July temperature of 11.1 °C (QMC-1). This T_{Jul} estimate is indicative of the Windermere Interstadial, a period of comparative climatic warmth and broadly equivalent to the GI-1 Interstadial (Coope and Pennington 1977; Walker and Lowe, 2019). The absence therefore of a robust cold climate indicator for the Dimlington Stadial, or a warming trend out of this phase is puzzling, but means that Quoyloo Meadow is similar to most other chironomid records in the British Isles. At present it is only the C-IT reconstructions from Whitrig Bog, Fiddaun and Lough Nadourcan which exhibit a proxy inferred thermal transition from the cold Dimlington Stadial, to the comparative warmth of the Windermere Interstadial (Brooks and Birks, 2000a; Van Asch *et al.*, 2012; Watson *et al.*, 2010). Why this should be is not immediately apparent, but the perseverance of 'dead-ice' within the basin and the inability to extrude the deepest sediments using Russian coring equipment, as suggested elsewhere (e.g. Brooks *et al.*, 2016), does not seem to be a viable explanation given the stratigraphic occurrence and estimated age of the Tanera Tephra.

At Quoyloo Meadow the first viable pollen counts ($n = 100$ total land pollen) were achieved at 223 cm with the occurrence of pioneering open-tundra grassland communities (QMP-1; 14.38 ± 0.73 to 14.1 ± 0.15 cal ka BP). This delayed colonization of Orkney, despite the chironomid data suggesting relatively high T_{Jul} from 237.5 cm (15.08 ± 1.58 cal ka BP), may relate to the local conditions. The most probable explanation is that retarded soil development and high wind-shear created instability in the catchment, which only ceased once pioneering taxa were able to stabilize the landscape. This instability and unfavourable conditions for higher plant colonization helps to explain why there is such a high rate of clastic sedimentation through the lower part of the record (Fig. 2), and also why the typical vegetation succession that occurred across Scotland during the Windermere Interstadial (e.g. *Rumex–Empetrum–Juniperus*; Walker *et al.*, 1994; Walker and Lowe, 2019) is not so readily observed on Orkney (e.g. Poaceae and *Empetrum*; Bunting, 1994; Abrook *et al.*, 2020a).

At 214.5 cm (14.04 ± 0.17 cal ka BP), the occurrence of cold-climate chironomid species increases (Fig. 4). Taxa such as *M. radialis*-type, *Sergentia coracina*-type, *H. grimshawi*-type *and P. sordidellus* suggest a short-term decline of 1.8 °C in T_{Jul} (12.4–10.6 °C; see QMC-e1 in Fig. 7) whilst increases of *Rheotanytarsus* and *Pseudosmittia* indicate a possible shallowing of the lake basin, expansion of the littoral zone and/or greater influence from stream input (Brooks *et al.*, 2007). Local changes are further reflected in the palynological record which records a shift to more open taxa at this time (216.5–210.5 cm; 14.09 ± 0.16–13.66 ± 0.90 cal ka BP; Abrook *et al.*, 2020a; Fig. 6). Following the perturbation, T_{Jul} recovers to around 14.1 °C (208.5 cm; 13.40 ± 1.10 cal ka BP) and vegetation communities stabilized (Fig. 6). Sedimentation rates reduced significantly through this interval, possibly caused by more dense and mature vegetation cover inhibiting the input of clastic materials into the basin. As a result, only 7 cm of sediment represents the period between the Penifiler Tephra (14.00 ± 0.16 cal ka BP) and the end of the Windermere Interstadial (13.06 ± 1.21 cal ka BP) at Quoyloo Meadow (Fig. 2).

Palaeoenvironmental changes during the Loch Lomond Stadial

Significant changes to the sediments and proxy series are noted at the transition from Unit 1c to Unit 2a (205.5 cm). The organic content of the silty-clay sediments decreases (208–200 cm; Fig. 2), charcoal frequency increases, and changes to the vegetation assemblage indicate the replacement of open heath vegetation (e.g. *Empetrum* and *Betula* cf. *nana*) by taxa more tolerant of cold and unstable conditions (e.g. *Salix*, Caryophyllaceae, Saxifragaceae and *Selaginella selaginoides*; Abrook *et al.*, 2020a; Fig. 6). The chironomid assemblage and C-IT reconstruction corroborates this inference of a cooler environment, cold-adapted species such as *M. radialis*-type, *P. austriacus*-type and *M. insignilobus*-type increase, and T_{Jul} falls from 12.0 to 6.0 °C (207.5–205.5 cm; 13.26 ± 1.17 to 13.00 ± 1.22 cal ka BP; Figs. 4 and 7). The timing of these changes, and the stratigraphic occurrence of the Vedde Ash at 198 cm (Timms *et al.*, 2017) confirms this interval as the Loch Lomond Stadial, a high-magnitude cold climate event broadly equivalent to the Younger Dryas and GS-1 interval (Lowe *et al.*, 2008, 2019; Walker and Lowe, 2019).

At 199.5 cm (12.20 ± 0.70 cal ka BP) just prior to the deposition of the Vedde Ash, T_{Jul} increases from 7.6 °C (201.5 cm) to 9.9 °C before returning to similarly low values shortly thereafter (6.8 °C; 197.5 cm; 11.93 ± 0.30 cal ka BP). This temporary increase in T_{Jul} coincides with a reduction of macro-charcoal and a change in vegetation communities. Xerophytic taxa such as *Artemisia* and instability indicators such as *Rumex* decrease, whilst *Empetrum* becomes more abundant. The expansion of heathland-type communities and a reduction in charcoal might suggest a brief interval of amelioration and one potentially typified by slightly wetter conditions.

Palaeoenvironmental changes during the early Holocene

The deposition of marl within the lacustrine environment at Quoyloo Meadow indicates increased catchment stability probably driven by rising temperatures. Calcium and bicarbonate supersaturation and precipitation in lake waters is temperature-dependent, and occurs once values reach approximately 10 °C (Kelts and Hsu, 1978; Cole and Weihe, 2015). At Quoyloo Meadow this thermal threshold is reached at the boundary between Units 2c and 3a (11.48 ± 0.48 cal a BP). This inference of amelioration is supported by the T_{Jul} reconstruction which shows a marked increase in temperatures from 6.7 to 12.4 °C (11.93 ± 0.30 to 11.16 ± 0.37 cal ka BP), along with the replacement of tundra-like plant communities with taxa such as *Rumex* and *Salix*. Collectively these indicators signal the onset of Holocene conditions.

Between 194 cm (11.44 ± 0.44 cal ka BP) and 184 cm (10.73 ± 0.23 cal ka BP) two minima in $\delta^{18}O$ values are observed (Fig. 5): QMO-e1 centred on 191.25 cm (11.13 ± 0.37 cal ka BP) and QMO-e2 centred on 186.25 cm (10.78 ± 0.18 cal ka BP). These low values are relatively subdued (<1‰) when compared to other $\delta^{18}O$ records of the period (e.g. Whittington *et al.*, 1996, 2015), but taken in isolation, it is possible that decreases of this scale could still reflect temperature oscillations in the order of 2–3 °C (Andrews, 2006; Candy *et al.*, 2011). Importantly, however, no such signal can be gleaned from the T_{Jul} reconstruction at the resolution undertaken, which shows a continued, if not a slightly slowed warming through this interval (QMC-2/3; Fig. 7). Low land-pollen concentrations and high levels of *Pediastrum* at the transition to the Holocene, and continuing during the QMO-e1 depletion, indicate a sparsely vegetated landscape prone to soil erosion (QMP-5; Abrook *et al.*, 2020a). This phase is succeeded by the establishment of a dwarf-shrub heathland (QMP-6), as well as a significant increase in the frequency of macro-charcoal fragments (Fig. 6). These latter changes coincide with the QMO-e2 isotopic depletion. With no clear fluctuation in the T_{Jul} reconstruction, it is possible that the $\delta^{18}O$ signal reflects changes to the hydrological regime as opposed to air temperature at this point of the record (Leng and Marshal, 2004). A more arid environment would probably have had a negligible impact on the pioneering vegetation established on the landscape during the QMO-e1 depletion, but following heathland development drier conditions during QMO-e2 may have led to drought stress (Bell and Tallis, 1973). This in turn may have increased the availability of biomass on the landscape, subsequently leading to an increase in fire frequency and charcoal production (Fig. 8). At present, our data cannot reconcile the significance of these isotopic excursions, especially with regard to aridity, but further research is addressing this.

Evidence between 184 cm (10.73 ± 0.23 cal ka BP) and 164 cm (10.28 ± 0.23 cal ka BP) indicates a phase of relative stability. Heathland taxa are gradually replaced by a herbaceous grassland, and T_{Jul} continues to rise, reaching a high of 15.6 °C at 168.5 cm (10.38 ± 0.27 cal ka BP) (Fig. 7). However, a number of minor perturbations are noted through this interval. At 174.5 cm (QMC-e2; 10.52 ± 0.32 cal ka BP) a reduction of 0.8 °C is inferred from the T_{Jul} reconstruction, and whilst no comparative oscillation can be identified in the isotope record, a slight inflection in the PrC dataset can be observed (Fig. 6). Closer scrutiny of the palynological record, however, illustrates that the PrC signal is probably responding to natural variability in the grassland communities (Abrook *et al.*, 2020a). Similarly, a minor depletion (<1‰) in the $\delta^{18}O$ record at 170.75 cm (QMO-e3; 10.43 ± 0.31 cal ka BP) has no proportional response in T_{Jul} or local vegetation communities. It is therefore probable that these minor perturbations in temperature and $\delta^{18}O$ values, if genuine, had a limited impact on the environment surrounding Quoyloo Meadow.

The most significant changes in the Quoyloo Meadow proxy series during the Holocene occur between 162.5 and 151.5 cm (10.25 ± 0.19 to 10.07 ± 0.21 cal ka BP) where T_{Jul} displays a two-stage drop in values (Fig. 7). An initial fall of 1.6 °C (162.5–161.5 cm; 10.25 ± 0.19 to 10.22 ± 0.16 cal ka BP) is followed by a temporary recovery, and a further decrease of 2.6 °C between 159.5 and 156.5 cm (10.19 ± 0.09 to 10.16 ± 0.11 cal ka BP; QMC-e3). Concurrent with this second reduction in temperature is a depletion in the $\delta^{18}O$ record of −0.52‰ (QMO-e4). The total drop in T_{Jul} of 3.75 °C is the largest seen in any Holocene oscillation identified in the British Isles (e.g. Lang *et al.*, 2010; Blockley *et al.*, 2018), and this factor, combined with the −0.52‰, suggests a significant shift in both mean annual and summer temperature variability that is further reflected in the vegetation assemblage. Retractions of *Empetrum* heath are apparent, and whilst grassland communities were already dominant on Orkney, elevated percentages of *Rumex* and increased macro-charcoal remains indicate a period of landscape reorganization, and greater incidences of burning (Abrook *et al.*, 2020a).

Following recovery from the preceding event, the rest of the studied Holocene sequence at Quoyloo Meadow shows no evidence of further short-lived fluctuations in climate. The prevalence of grassland communities is gradually reduced as woody vegetation such as *Betula* and *Corylus* becomes more established, and temperatures remain stable.

Discussion

Short-lived 'centennial' climate oscillations

The precision of the Quoyloo Meadow age-model offers an excellent opportunity to make an independent chronological comparison of the proxy series to the NGRIP regional stratotype (Fig. 8). Centennial-scale climatic events have been identified where a change is recorded across multiple lines of palaeoclimatic evidence, or where a change is recorded in a single proxy or data-point, and reasonable justification can be made as to why this may not be reflected in other data series or surrounding datum (Table 2; Fig. 8). Here we consider the timing and regionality of the short-lived climatic events described from Quoyloo Meadow with a specific emphasis on the early Holocene.

Late Pleistocene oscillations (QMC-e1)

The reduction in mean July temperatures observed at Quoyloo Meadow (*c.* 214.5 cm; QMC-e1; Fig. 7) during the early Windermere Interstadial (*c.* GI-1), and the shift to more open-habitat taxa, is an event that is also recorded in other lacustrine

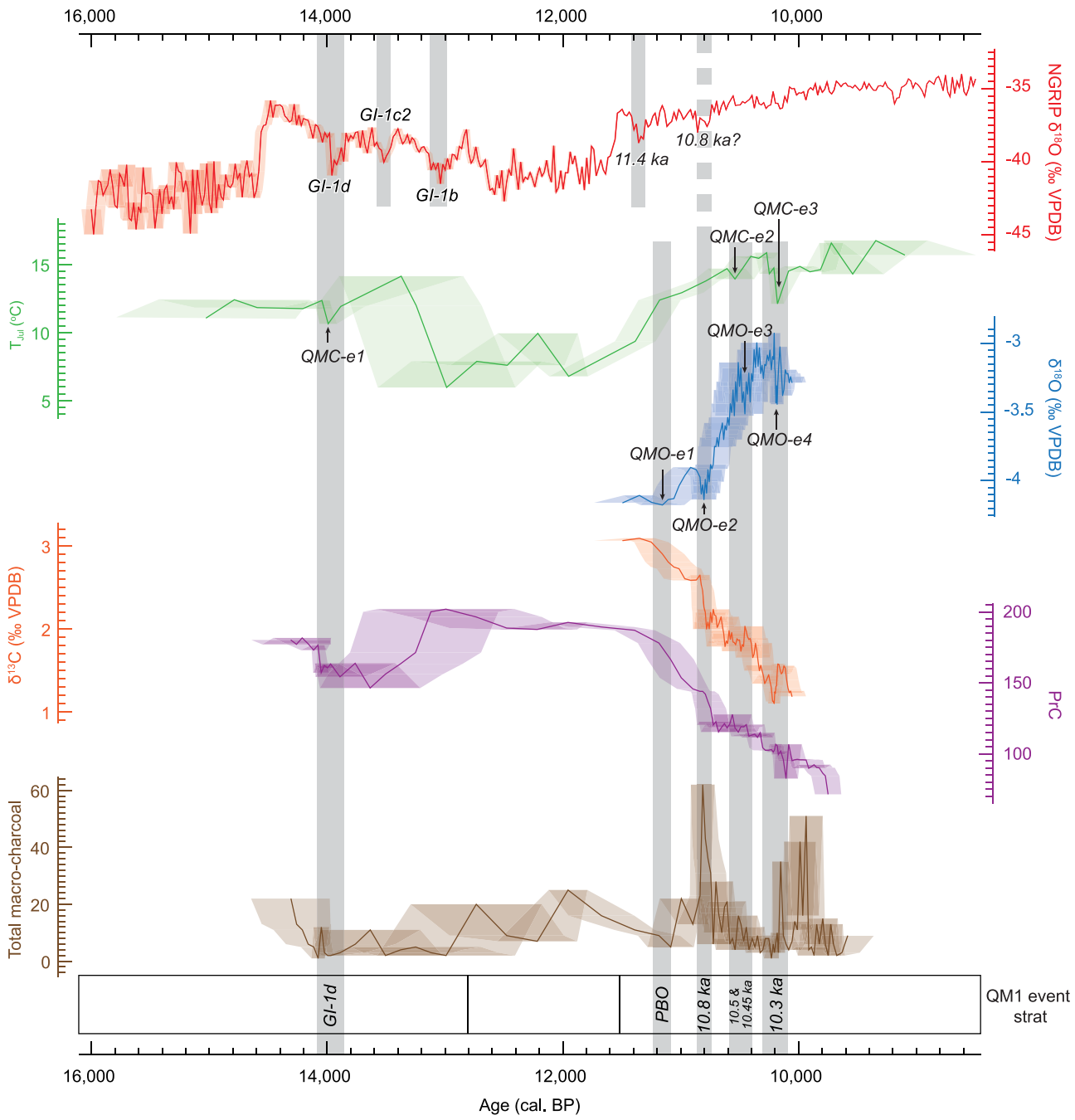

Figure 8. A chronological comparison of the Quoyloo Meadow proxy series with the NGRIP $\delta^{18}O$ regional stratotype. Both records are plotted on a common chronological scale with the coloured 'blurring' illustrating a one sigma uncertainty. Within this uncertainty a correlation can be made between QMC-e1 and GI-1d. Throughout the early Holocene, the Quoyloo Meadow proxy series exhibits a series of 'events' which have no clear analogue within the ice-core record. A possible exception to this is an event at *c.*10.8 ka, but the possible corresponding oscillation in the NGRIP record has yet to be formally recognized by the ice-core community. This difference between Quoyloo Meadow and NGRIP during the early Holocene suggests the Orkney Isles were responding to forcing factors that were either different from those operating over Greenland, or were more strongly manifest at mid-latitude sites. NGRIP data are from Rasmussen *et al.* (2014). [Color figure can be viewed at wileyonlinelibrary.com].

Table 2. Summary of centennial-scale events identified within the chironomid and stable isotope data at Quoyloo Meadow. Ages are approximate only; see main text for full age-error estimates

Approximate age (cal ka BP)	Chironomid events	Isotopic events
14.0	QMC-e1	n/a
11.1	no signal	QMO-e1
10.8	no signal	QMO-e2
10.5	QMC-e2	no signal
10.45	no signal	QMO-e3
10.3	QMC-e3	QMO-e4

records across NW Europe (e.g. Brooks and Langdon, 2014; Heiri *et al.*, 2014; Moreno *et al.*, 2014). In the regional Greenland stratotype, three short-lived centennial-scale oscillations have been recorded in the GI-1 interval: GI-1d, GI-1c and GI-1b (Johnsen *et al.*, 1992; Björck *et al.*, 1998; Rasmussen *et al.*, 2014). Determining their chrono-stratigraphic equivalence in terrestrial records has, however, proved problematic due to uncertainties associated with site-specific age-models and the comparability between different proxy series (Lowe and Walker, 2000; Blaauw *et al.*, 2007; Blaauw, 2012). At Quoyloo Meadow, correlation is assisted by the Borrobol (218 cm) and Penifiler (213 cm) tephras, two isochronous markers which bracket the onset and termination

of QMC-e1. The precise age estimate for these tephra (see Table 1) provides a well-constrained age for the climatic oscillation (14.04 ± 0.17 cal ka BP), which, if the error range is taken into account, falls within the ice-core age span of 14.08–13.94 b2k for the GI-1d oscillation (Rasmussen *et al.*, 2014). On this basis, and given the relationship of these well-dated tephra with temperature responses identified elsewhere (e.g. Matthews *et al.*, 2011; Brooks *et al.*, 2012; Brooks *et al.*, 2016; Candy *et al.*, 2016), we propose that the oscillation detected at Quoyloo Meadow is the equivalent of the GI-1d cooling event in the Greenland ice-core record (Fig. 8). Unfortunately, the limited stratigraphic resolution afforded by the Quoyloo Meadow record through units 1b and 1c (Fig. 2) means that it is difficult to compare the magnitude of this cooling (*c.* 1.7 °C) with other contemporaneous records. Recourse to other sequences which have the capacity to be resolved to a higher resolution, e.g. Crudale Meadow (Whittington *et al.*, 2015; Timms *et al.*, 2018) and Loch of Sabiston (Cochrane, 2020), may offer a better opportunity for further study of this event on Orkney.

Early Holocene oscillations (QMO-e1, e2 and e4; QMC-e3 and e4)

During the early Holocene, the Greenland $\delta^{18}O$ trend is characterized by gradually increasing isotopic values (Vinther *et al.*, 2006; Rasmussen *et al.*, 2007; Fig. 8). Punctuating this trend, however, are a number of major isotopic excursions, the 11.4-ka event, the 9.3-ka event and the 8.2-ka event (Rasmussen *et al.*, 2007). These events are consistently expressed in DYE-3, GRIP and NGRIP, and hence represent regionally if not hemispherically significant climatic oscillations (Rasmussen *et al.*, 2007; Walker *et al.*, 2019). Some of these events have been identified in European proxy records, but correlation with the Greenland ice-core sequence is uncertain, particularly the 11.4-ka event which has been linked, perhaps incorrectly, with the European Pre-Boreal Oscillation (PBO) (Björck *et al.*, 1996). The PBO, dated to *c.* 11.2 ka, has been evidenced through greater winter–summer seasonality, a reversion to grassland-type communities and a widespread drying of the climate (van der Plicht *et al.*, 2004; Andresen *et al.*, 2007; Bohncke and Hoek, 2007; Bos *et al.*, 2007; Jessen *et al.*, 2008; Wohlfarth *et al.*, 2017). Chronological uncertainty and variable stratigraphic resolution, however, inhibit establishing the synchroneity of these responses, and whether they can be attributed to the same forcing factors operating over Greenland at this time. It is thus unclear whether the PBO and the 11.4-ka event represent either a single synchronous event, or a temporally and spatially transgressive event, or whether the 11.4-ka event and PBO represent different episodes over Greenland and Europe. It should also be noted that the PBO fits into a broader period of climatic instability described from European sequences dating to between *c.* 11.25 and 10.5 ka, but which seemingly have no clear analogue within the Greenland ice-core records (Diefendorf *et al.*, 2006; Andresen *et al.*, 2007; Jessen *et al.*, 2008; Fiłoc *et al.*, 2018 and references therein).

The Quoyloo Meadow record matches with this continental-wide pattern of early Holocene climatic instability. Isotopic events QMO-e1 (11.13 ± 0.37 cal ka BP) and QMO-e2 (10.78 ± 0.18 cal ka BP) coincide with phases of vegetational change (QMP-5/6; Fig. 6), and increased macro-charcoal is associated with QMO-e2 (Fig. 8). As far as the resolution of the reconstruction allows there is no discernible T_{Jul} response associated with these isotopic events at Quoyloo Meadow. This suggests summer temperature change was not a major component affecting the records, and instead implicates aridity and/or greater winter temperature ranges as principal forcing factors (e.g. Björck *et al.*, 1997; Denton *et al.*, 2005). Indeed, the impact of winter as opposed to summer conditions as drivers of abrupt early Holocene changes has been suggested by a range of data from other sites in Greenland (Andresen *et al.*, 2007), the Faroes (Andresen *et al.*, 2007; Jessen *et al.*, 2008), the Netherlands (van der Plicht *et al.*, 2004; Bohncke and Hoek 2007; Bos *et al.*, 2007), Germany (Mekhaldi *et al.*, 2019) and the British Isles (Blockley *et al.*, 2018; Abrook *et al.*, 2020b). However, summer temperature variability cannot be excluded entirely, as C-IT reconstructions from Star Carr, England, show reductions contemporaneously with isotopic events at 11.4 and 11.1 ka BP (Blockley *et al.*, 2018). Quoyloo Meadow also exhibits summer temperature variability in the early Holocene, but this does not occur until QMC-e2 (10.52 ± 0.32 cal ka BP; Fig. 7). The timing of QMC-e2 and the preceding isotopic events at Quoyloo Meadow, means that, within chronological error, broad correlations can be drawn to the PBO and other phases of environmental instability recorded in European archives at approximately 11.1 (QMO-e1), 10.8 (QMO-e2), 10.5 (QMC-e2) and 10.45 (QMO-e3) cal ka BP (Fig. 8).

Between 10.25 ± 0.19 and 10.07 ± 0.21 cal ka BP the palaeoenvironmental archive at Quoyloo Meadow records its most distinct response to centennial-scale climate forcing. A strong isotopic excursion (QMO-e4), a reduction in T_{Jul} estimates (QMC-e3), and a greater presence of open ground vegetation (QMP-8/9) suggests a major disruption to the local environment (Fig. 8). The precise timing of this event is constrained by the Saksunarvatn Ash and Fosen Tephra, two isochronous markers which act as a distinct tephra couplet within the Holocene (Lind *et al.*, 2013; Timms *et al.*, 2017, 2019). Whilst studies have questioned the chemical uniqueness, and hence validity of the Saksunarvatn Ash as an isochronous marker (Davies *et al.*, 2012; Jennings *et al.*, 2014; Óladóttir *et al.*, 2020), we have found no conclusive evidence of contemporaneous basaltic ash layers (see QM1 175 and 170 in Timms *et al.*, 2017), nor did we identify glass shards bearing low MgO wt% values within our chemical analyses; the latter is a distinctive characteristic of other 'Saksunarvatn-like' tephras deposited within the same time-frame (*c.* 10.5–9.9 ka BP; Wastegård *et al.*, 2018). We therefore consider the 'Saksunarvatn Ash' to be a reliable stratigraphic and chronological tie-point within the Quoyloo Meadow record. The Saksunarvatn Ash has previously been associated with a climatic perturbation termed the '10.3-ka event' (Björck *et al.*, 2001; Andresen *et al.*, 2007). Evidence for this oscillation has principally come from archives in Europe and North America, which show a significant environmental disturbance at this time (Table 3). On the basis of the tephra evidence and the magnitude of the proxy response at Quoyloo Meadow, we propose a correlation to this event.

In the British Isles very few early Holocene centennial-scale climatic perturbations have been reliably described or dated, and emphasis has historically been placed on providing evidence for the PBO, 9.3-ka and 8.2-ka events (e.g. Whittington *et al.*, 1996, 2015; Diefendorf *et al.*, 2006; Marshall *et al.*, 2002, 2007; Lang *et al.*, 2010; Holmes *et al.*, 2015, 2020; Blockley *et al.*, 2018). These events are the largest, most widely detected and often considered the most important in understanding early Holocene climatic complexity. However, these events are only part of the complexity, and a tendency to focus on them has masked the intricacy of local–regional expressions of climate change following large-scale reorganization of the ocean–atmospheric system. The evidence presented here would suggest that the event recorded at *c.* 10.3–10.0 cal ka BP had a greater impact on the climate

Table 3. Compilation of palaeoenvironmental site data for which there is evidence of a temperature decline and/or environmental fluctuation at approximately 10.3 ka BP. The present distribution of evidence would suggest that the 10.3-ka event is infrequently identified in palaeoclimate sequences, and those where it has been found are preferentially located in northern Europe and North America, suggesting an oceanic (North Atlantic) origin, or mechanism of propagation. Data have been primarily extracted from Kaufman *et al.* (2020) and references therein

Region	Site	Approximate age	Proxy evidence	Oscillation commented upon in text (Y/N)	References	Latitude (°)	Longitude (°)	Elevation (m)
Greenland	GRIP	*c.* 10 300 cal a BP	$\delta^{18}O$ minimum at *c.* 10.3 cal ka BP.	Y	Björck *et al.* (2001)	72.579	−37.565	3238
North Atlantic	VM 28-14	*c.* 10 400 cal a BP	Enhanced ice-rafting episodes (IRD7), lower sea surface temperatures, and a minimum in $\delta^{13}C$ values suggest a reduction in NADW formation.	Y	Bond *et al.* (1997)	64.786	−29.569	−1855
	VM 29-191	*c.* 10 300 cal a BP		Y		54.269	−16.786	−2370
Faroe Islands	Lake Starvatn	10 350-10 300 cal a BP	Multiproxy evidence: Reduction in birch and increases in grass and herb pollen suggest a cooling of the climate. Decreased aquatic productivity due to prolonged ice-cover is also indicated along with increased soil erosion in the catchment.	Y	Björck *et al.* (2001)	62.085	−6.722	116
	Lykkjuvøtn	*c.* 10 300 cal a BP.	Modest response in winter sea ice cover and reduced diatom productivity. Possible increase in catchment erosion.	Y	Jessen *et al.* (2008)	61.889	−6.867	125
Norwegian Sea	HM79-6	*c.* 10 300 cal a BP	Sea surface temperature (SST) minimum indicates a summer temperature drop of 2.7 °C, and winter SST drop of 2.1 °C.	Y	Karpuz and Jansen, (1992); Björck *et al.* (2001)	62.967	2.700	–
Norway	Sunnmøre	10 450-10 005 cal a BP	Glacial readvance and moraine formation.	Y	Dahl *et al.* (2002)	Several localities, see references for details		
	Jostedalsbreen	10 300-9900 ca a BP, 10 100–10 050 cal a BP and *c.* 9700 cal a BP	Several outlet glaciers of the Jostedalsbreen ice-cap, including at the type site Erdalen, experienced a two-stage glacial readvance marked by moraine formation. Age estimates for re-advance vary between outlet glaciers.	Y	Nesje *et al.* (1991); Dahl *et al.* (2002)	Several localities, see references for details		
	Sognefjell	*c.* 10 200–9700 ka	Glacial readvance and moraine formation.	Y	Shakesby *et al.* (2020)	Several localities, see references for details		
	Styggedalsbreen	*c.* 10 200–9700 ka	Glacial readvance and moraine formation.	Y		Several localities, see references for details		
	Kråkenes	*c.* 10 300 cal a BP	Fluctuations in the C-IT reconstruction occur around deposition of Saksunarvatn Ash, but there is no clear reduction in temperature.	N	Brooks and Birks (2000b)	62.027	5.004	40
	Myklevatnet	10 200 b2k	C-IT reconstruction suggests a 1.2 °C decline around 10 200 b2k. A corresponding increase in Ti values might suggest greater catchment instability.	Y	Nesje *et al.* (2014)	61.920	5.221	123
	Vestre Øykjamyrtjørn	*c.* 10 300 cal a BP	C-IT reconstruction hints at a possible reduction of *c.* 2 °C around 10.3 cal ka BP.	N	Velle *et al.* (2005)	59.820	6.000	570
Finland	Sokli	*c* 10 200 cal a BP	C-IT reconstruction exhibits a decline of *c.* 1.4 °C between 10.4 and 10.2 cal ka BP	N	Shala *et al.* (2017)	67.810	29.280	220
British Isles	Quoyloo Meadow	*c.* 10 300–10 000 cal a BP	Two-stage oscillation characterized by an enrichment in $\delta^{18}O$ values, a shift in vegetational communities to those indicative of a 'less-stable' climatic regime, and a reduction in C-IT (total magnitude 3.75 °C).	Y	This study	59.066	−3.309	30

(*Continued*)

Table 3. (*Continued*)

Region	Site	Approximate age	Proxy evidence	Oscillation commented upon in text (Y/N)	References	Latitude (°)	Longitude (°)	Elevation (m)
	Haweswater	*c.* 10 400–10 300 cal a BP	Two-stage oscillation suggests a cooling of mean summer temperatures by *c.* 1.2 °C.	Y	Lang *et al.* (2010)	54.183	−2.800	8
Spain	Salines playa lake	*c.* 10 300 cal a BP	Several pollen-inferred aridity events are noted in the early Holocene, including one at *c.* 10.3 cal ka BP.	Y	Burjachs *et al.* (2016)	38.505	−0.892	475
Switzerland	Eglesee	*c.* 10 400– 10 000 cal a BP	C-IT reconstruction shows a reduction of *c.* 1.7 °C between 10.4 and 10.0 cal ka BP	N	Larocque-Tobler *et al.* (2010)	47.180	8.580	770
	Hinterburgsee	*c.* 10 400 cal a BP	C-IT reconstruction shows a reduction of *c.* 1.7 °C centred on *c.* 10.4 cal ka BP	Y	Heiri *et al.* (2003)	46.718	8.068	1515
	Foppe	*c.* 10 300 cal a BP	C-IT reconstruction shows a reduction of *c.* 1.5 °C centred on *c.* 10.3 cal ka BP	N	Samartin *et al.* (2012)	46.460	8.794	1470
Poland	Żabieniec bog	*c.* 10 300 cal a BP	C-IT reconstruction using the Swiss training set shows a reduction in temperature of *c.* 2 °C. A reduction, albeit smaller in magnitude, is also noted using the Norwegian training set. No reduction is noted using the Russian training set	N	Płóciennik *et al.* (2011)	51.852	19.781	180
Romania	Lake Brazi	10 350–10 190 cal a BP	C-IT reconstruction shows a drop in mean summer temperatures of *c.* 1.4 °C possibly accompanied by a rapid lowering of lake levels.	Y	Tóth *et al.* (2015)	45.396	22.902	1740
Russia	Lyadhej-To	*c.* 10 340 cal a BP	C-IT reconstruction shows a reduction in summer temperature of *c.* 1.9 °C at 10.3 cal ka BP	N	Andreev *et al.* (2005)	68.260	65.800	150
	Kharinei	*c.* 10 100 cal a BP	C-IT reconstruction shows a decline in summer temperature estimates of *c.* 2 °C centred on 10.1 cal ka BP	N	Jones *et al.* (2011)	67.363	62.751	108
North America	Labrador dome	*c.* 10 400 cal a BP	Labrador dome moraine development suggests stability of the ice-cap	Y	Ulmman *et al.* (2016)	Several localities, see references for details		
	Screaming Lynx Lake	*c.* 10 400 cal a BP	C-IT reconstruction shows a decline of *c.* 0.75 °C centred on 10.40 cal ka BP	N	Clegg *et al.* (2011)	64.206	−145.814	293
	Rainbow lake					66.067	−145.400	223
	Lake of the Woods	*c.* 10 300 cal a BP	C-IT reconstruction shows a decline of *c.* 1.0 °C centred on 10.38 cal ka BP	N	Palmer *et al.* (2002)	49.050	−120.183	2050

and landscape of Orkney than any other early Holocene event recorded in the British Isles. The magnitude is approximately double the impact of the PBO recorded at Star Carr (Blockley *et al.*, 2018) and approximately 1.7 °C greater than the 9.3-ka event described from Haweswater (Lang *et al.*, 2010). Whilst an oscillation at *c.* 10.3 ka has been noted at Haweswater (Table 3), it is comparatively subdued when compared to the Quoyloo Meadow record. Why this should be is not immediately clear, and why this event should remain undetected in other climate archives across the British Isles is also uncertain. A possible explanation is that there was a strong latitudinal gradient related to the impact of this event similar to other climatic transitions detected in the British Isles (e.g. Coope *et al.*, 1998; Isarin and Bohncke, 1999; Brooks and Langdon, 2014), and that many climate records that span this interval have not been investigated to a sufficiently high resolution as to detect change.

Climatic drivers in the early Holocene

Freshwater fluxes into the North Atlantic during the early Holocene have long been considered as possible driving mechanisms behind abrupt climate variability (Clark *et al.*, 2001; Fisher *et al.*, 2002; Teller *et al.*, 2002; Nesje *et al.*, 2004). Specifically, multiple outpourings of glacial lake Agassiz–Ojibway into the Atlantic, and periodic drainage of the Baltic are linked to episodes of climate variability dating to between *c.* 11.7 and 9.0 cal ka BP (Björck *et al.*, 1996; Bodén *et al.*, 1997; Teller *et al.*, 2002; Jessen *et al.*, 2008; Smith *et al.*, 2011). Influxes of fresh water disrupted Atlantic meridional overturning (AMOC), forcing polar waters southwards through increased ocean stratification and inhibiting the northerly advection of heat in the Atlantic Ocean (Björck *et al.*, 1996; Bond *et al.*, 1997; Fisher *et al.*, 2002; Andresen *et al.*, 2007). The 10.3-ka event can therefore be potentially linked to drainage of the lake Agassiz McCauleyville stage (Teller *et al.*, 2002), as well as to a near simultaneous outpouring of the Nedre Glamsjø lake in Norway (*c.* 10.3 cal ka BP; Longva and Thoresen, 1991; Nesje *et al.*, 2004). The 10.3-ka event was perhaps further influenced by the drainage of the Baltic Ancylus lake shortly thereafter at *c.* 10.16–9.8 cal ka BP (Björck, 1995; Nesje *et al.*, 2004). The combined impacts of these 'freshening' episodes spanning *c.* 10.3–9.8 ka BP may have been enough to weaken AMOC and trigger a cooling episode across much of the Northern Hemisphere. In Scandinavia a multi-stage glacial readvance, known locally as the 'Erdalen' events (Nesje *et al.*, 1991; Dahl *et al.*, 2002; Matthews *et al.*, 2008; Shakesby *et al.*, 2020; Table 3), has been attributed to an increase in winter precipitation and by a significant drop in summer temperatures at this time (Dahl *et al.*, 2002). Contemporaneous records from across Europe, North America and the North Atlantic agree with this, and suggest a period of environmental instability, reduced catchment productivity and an increase in ice-rafted debris (IRD event 7) accompanied the shift in temperatures (Table 3; Bond *et al.*, 1997; Björck *et al.*, 2001).

An alternative explanation for short-term climate cooling in the early Holocene, other than meltwater, is the role of solar forcing. Evidence of ^{10}Be and ^{14}C fluctuations in ice-core and tree-ring records, respectively, suggest that a number of climatic events identified through the early Holocene coincide with solar events (Bond *et al.*, 2001; Muscheler *et al.*, 2004; Adolphi *et al.*, 2014). This mechanism has previously been used to explain the origin of the 10.3-ka event (Björck *et al.*, 2001), and may have been a more prominent contributor to early Holocene climate variability than previously thought (Jessen *et al.*, 2008). This mechanism has also recently been invoked by Mekhaldi *et al.* (2019) to explain why the PBO appears greater in magnitude and extent than later early Holocene events. A solar minimum coinciding with the PBO is suggested to have 'pre-conditioned' the climate so that it was more susceptible to episodes of meltwater flux. By contrast the 10.3-ka event, whilst also associated with major glacial-lake drainage episodes, had not been 'pre-conditioned' by a solar minimum, but instead occurred at a time of heightened solar activity, effectively muting the signal of the outburst floods. Hence, the 10.3-ka event is less well represented in palaeoclimate records when compared to the PBO phase of instability (Mekhaldi *et al.*, 2019).

At Quoyloo Meadow, however, this is not the case, with the 10.3-ka event notably more pronounced than any preceding short-lived oscillation of the early Holocene, and represented quite clearly by a two-stage structure in mean July temperature (Fig. 7). The later and larger reduction has a coeval response in δ^{18}O values, which perhaps suggests the influence of two or more forcing episodes or a divergence between summer and mean annual temperature signals. Whilst speculative, the two-stage proxy response detected at Quoyloo Meadow might suggest that an initial meltwater outpouring had only a minimal impact on mean summer temperatures across Orkney, allowing the islands to return temporarily to a stabilized state shortly thereafter. This was followed by a further event(s) which may be represented in the Quoyloo Meadow record by the larger secondary oscillation detected in both the C-IT and δ^{18}O records, summer and mean annual indicators respectively. The divergence in proxy response observed may relate to: (i) the magnitude of the outburst floods; (ii) the proximity of the events in relation to the Orkney Isles; (iii) the condition of AMOC at the time; and/or (iv) the susceptibility of the Orkney Isles to change (i.e. how close the system was to climate and environmental thresholds). It is probable that a weakened AMOC from the accumulative effects of several closely timed outpourings may have facilitated a stronger response than expected from a single event, and due to the more 'proximal' location of Orkney and the Faroes to the North Atlantic, this was preferentially recorded here as a larger magnitude event when compared with records from other areas of NW Europe.

Conclusions

The tephrochronological approach adopted and the updated tephra age estimates presented here enable a decadal-level of chronological precision which could not have been achieved at Quoyloo Meadow with radiometric techniques alone. This demonstrates that tephrochronology is a valuable means by which chronologies can be developed in traditionally 'hard-to-date' sequences such as carbonate precipitating lakes and those devoid of plant macrofossils for radiocarbon dating. With the number of well-dated (crypto-)tephra that are known to be present in palaeoenvironmental and archaeological records (e.g. Davies *et al.*, 2012; Blockley *et al.*, 2014; Timms *et al.*, 2019), we echo previous calls and recommend this approach be adopted more widely to develop and supplement chronologies from other sequences across the British Isles and NW Europe that span the LGIT.

The Quoyloo Meadow proxy series provides further insight into the climatic variability of northern Britain during the LGIT. In particular, the study presents new biostratigraphic and isotopic data to support evidence of multiple short-lived climatic reversal events impacting the Orkney Isles (see Whittington *et al.*, 2015; Abrook *et al.*, 2020a). These events can be shown to be broadly equivalent to the widely recognized GI-1d and PBO phases of instability. However,

we also identify, with varying degrees of confidence, evidence for further climatic instability during the Holocene and dating to *c.* 10.8, 10.5, 10.45 and 10.3 cal ka BP.

The evidence from Quoyloo Meadow shows that the most pronounced cooling event, other than the Loch Lomond Stadial, occurred between *c.* 10.3 and 10.0 cal ka BP which is indicated by a drop of 3.75 °C in mean July temperatures, a shift in vegetational communities to those indicative of 'less stable' climatic regimes, and a decrease in $\delta^{18}O$ values. We interpret this as evidence of the '10.3 ka event', a climatic perturbation infrequently identified in early Holocene palaeoenvironmental reconstructions, and is the first reliably dated incidence of this event in the British Isles. This is a significant finding as the magnitude of the event in the Orkney record is considerably larger than any other early Holocene perturbation detected in the British Isles to date. However, we cannot exclude the fact that this magnitude of response may reflect factors either unquantified in the current study or unique to Quoyloo Meadow itself.

The results from Quoyloo Meadow show that not only the LGIT, but also the early Holocene, were both dynamic and complex intervals of climatic and environmental change. Despite research into many LGIT and early Holocene sequences from the British Isles, detecting the exact frequency and magnitude of climatic events remains difficult. Continuing to develop similar records with high chronological precision combined with high stratigraphic resolution will enable better understanding of abrupt climatic events in terrestrial records across NW Europe during these key time intervals. While the Greenland ice-core records continue to be the stratigraphic template for the North Atlantic region, it now seems that they do not exhibit all of the events being discovered in terrestrial palaeoclimate records in Europe. The identification of centennial-scale events such as GI-1d or the PBO, with a wide geographical range, is well known, but the Quoyloo Meadow record has shown that it is also possible to detect more spatially restricted events. Understanding why these events are expressed in this manner, when their driving mechanisms appear to be similar to those that are more strongly represented, is a clear priority for future investigations.

Supporting information

Additional supporting information may be found in the online version of this article at the publisher's web-site.

Supplementary Table S1. Quoyloo Meadow chironomid data.

Supplementary Table S2. sedimentological description of the Quoyloo Meadow (QM1) composite core.

Supplementary Table S3. Quoyloo Meadow proxy & chrono data.

Acknowledgements. The authors would like to acknowledge Orkney Brewery for access to the Quoyloo Meadow site and thank Dr Stefan Engels (Birkbeck) for his assistance with the chironomid identifications and interpretation. Thanks are also owed to Professor Oliver Heiri (Basel) and co-workers for making the combined Swiss–Norwegian calibration dataset available online. Gratitude is further extended to Professor Mike Walker and an anonymous reviewer for their helpful comments and constructive feedback on an earlier version of the manuscript. R.T. would like to thank the QRA for a New Researchers Worker Award that part-funded the coring campaign in February 2014. A.A. was supported by the Natural Environmental Research Council (Grant number NE/L002485/1) during the completion of this work. The authors confirm no conflicts of interest.

Data availability statement

The data that support the findings of this study are available in the online Supporting Information.

References

Abrook AM, Matthews IP, Milner AM, Candy I, Palmer AP, Timms RG. 2020a. Environmental variability in response to abrupt climatic change during the Last Glacial–Interglacial Transition (16–8 cal ka BP): evidence from Mainland, Orkney. *Scottish Journal of Geology* **56**: 30–46.

Abrook AM, Matthews IP, Candy I, Palmer AP, Francis CP, Turner L, Brooks SJ, Self AE, Milner AM. 2020b. Complexity and asynchrony of climatic drivers and environmental responses during the Last Glacial-Interglacial Transition (LGIT) in north-west Europe. *Quaternary Science Reviews* **106634**.

Adolphi F, Muscheler R, Svensson A, Aldahan A, Possnert G, Beer J, Sjolte J, Björck S, Matthes K, Thiéblemont R. 2014. Persistent link between solar activity and Greenland climate during the Last Glacial Maximum. *Nature Geoscience* **7**(9): 662–666.

Andreev AA, Tarasov PE, Ilyashuk BP, Ilyashuk EA, Cremer H, Hermichen WD, Wischer F, Hubberten HW. 2005. Holocene environmental history recorded in Lake Lyadhej-To sediments, polar Urals, Russia. *Palaeogeography, Palaeoclimatology, Palaeoecology* **223**(3-4): 181–203.

Andresen CS, Björck S, Jessen C, Rundgren M. 2007. Early Holocene terrestrial climatic variability along a North Atlantic Island transect: palaeoceanographic implications. *Quaternary Science Reviews* **26**: 1989–1998.

Andrews JE. 2006. Palaeoclimatic records from stable isotopes in riverine tufas: synthesis and review. *Earth-Science Reviews* **75**(1): 85–104.

Baillie MGL. 1991. Suck-in and smear: two related chronological problems for the 90 s. *Journal of theoretical archaeology* **2**: 12–16.

Bell JNB, Tallis JH. 1973. Empetrum nigrum L. *Journal of Ecology* **61**(1): 289–305.

Birks HJB. 1998. Numerical tools in palaeolimnology- progress, potentialities, and problems. *Journal of Paleolimnology* **20**: 307–332.

Birks HJB, Heiri O, Seppä H, Bjune AE. 2010. Strengths and weaknesses of quantitative climate reconstructions based on Late-Quaternary. *The Open Ecology Journal* **3**: 1.

Bjorck S, Kromer B, Johnsen S, Bennike O. 1996. Synchronized terrestrial-atmospheric deglacial records around the North Atlantic. *Science* **274**(5290): 1155–1160.

Björck S, Rundgren M, Ingolfsson Ó, Funder S. 1997. The Preboreal oscillation around the Nordic Seas: terrestrial and lacustrine responses. *Journal of Quaternary Science* **12**(6): 455–465.

Björck S, Walker MJ, Cwynar LC, Johnsen S, Knudsen KL, Lowe JJ, Wohlfarth B. 1998. An event stratigraphy for the Last Termination in the North Atlantic region based on the Greenland ice-core record: a proposal by the INTIMATE group. *Journal of Quaternary Science* **13**(4): 283–292.

Björck S, Muscheler R, Kromer B, Andresen CS, Heinemeier J, Johnsen SJ, Conley D, Koç N, Spurk M, Veski S. 2001. High-resolution analyses of an early Holocene climate event may imply decreased solar forcing as an important climate trigger. *Geology* **29**(12): 1107–1110.

Blaauw M. 2012. Out of tune: the dangers of aligning proxy archives. *Quaternary Science Reviews* **36**: 38–49.

Blaauw M, Christen JA, Mauquoy D, van der Plicht J, Bennett KD. 2007. Testing the timing of radiocarbon-dated events between proxy archives. *The Holocene* **17**(2): 283–288.

Blockley SP, Bourne AJ, Brauer A, Davies SM, Hardiman M, Harding PR, Lane CS, MacLeod A, Matthews IP, Pyne-O'Donnell SD, Rasmussen SO, Wulf S, Zanchetta G. 2014. Tephrochronology and the extended intimate (integration of ice-core, marine and terrestrial records) event stratigraphy 8–128 ka b2k. *Quaternary Science Reviews* **106**: 88–100.

Blockley S, Candy I, Matthews I, Langdon P, Langdon C, Palmer A, Lincoln P, Abrook A, Taylor B, Conneller C, Bayliss A, McLeaod A, Deeprose L, Darvill C, Kearney R, Beavan N, Staff R, Bamforth M,

Taylor M, Milner N. 2018. The resilience of postglacial hunter-gatherers to abrupt climate change. *Nature ecology & evolution* **2**(5): 810–818.

Bodén P, Fairbanks RG, Wright JD, Burckle LH. 1997. High-resolution stable isotope records from southwest Sweden: the drainage of the Baltic Ice Lake and Younger Dryas Ice Margin Oscillations. *Paleoceanography* **12**(1): 39–49.

Bohncke SJP, Hoek WZ. 2007. Multiple oscillations during the Preboreal as recorded in a calcareous gyttja, Kingbeekdal, The Netherlands. *Quaternary Science Reviews* **26**(15-16): 1965–1974.

Bond G, Showers W, Cheseby M, Lotti R, Almasi P, DeMenocal P, Priore P, Cullen H, Hajdas I, Bonani G. 1997. A pervasive millennial-scale cycle in North Atlantic Holocene and glacial climates. *Science* **278**(5341): 1257–1266.

Bond G, Kromer B, Beer J, Muscheler R, Evans MN, Showers W, Hoffmann S, Lotti-Bond R, Hajdas I, Bonani G. 2001. Persistent solar influence on North Atlantic climate during the Holocene. *Science* **294**(5549): 2130–2136.

Bos JA, van Geel B, van der Plicht J, Bohncke SJ. 2007. Preboreal climate oscillations in Europe: wiggle-match dating and synthesis of Dutch high-resolution multi-proxy records. *Quaternary Science Reviews* **26**(15-16): 1927–1950.

Broecker WS, Denton GH. 1990. The role of ocean-atmosphere reorganizations in glacial cycles. *Quaternary Science Reviews* **9**(4): 305–341.

Bronk Ramsey C. 2008. Deposition models for chronological records. *Quaternary Science Reviews* **27**(1-2): 42–60.

Bronk Ramsey C. 2017. Oxcal Version 4.3.2 https://c14.arch.ox.ac.uk/oxcal/OxCal.html [Software]

Bronk Ramsey C, Lee S. 2013. Recent and planned developments of the program OxCal. *Radiocarbon* **55**(2-3): 720–730.

Brooks SJ, Birks HJB. 2000a. Chironomid-inferred Late-glacial air temperatures at Whitrig Bog, Southeast Scotland. *Journal of Quaternary Science* **15**(8): 759–764.

Brooks SJ, Birks HJB. 2000b. Chironomid-inferred late-glacial and early-Holocene mean July air temperatures for Kråkenes Lake, western Norway. *Journal of Paleolimnology* **23**(1): 77–89.

Brooks SJ, Birks HJB. 2001. Chironomid-inferred air temperatures from Lateglacial and Holocene sites in north-west Europe: Progress and problems. *Quaternary Science Reviews* **20**(16–17): 1723–1741.

Brooks SJ, Heiri O. 2013. Response of chironomid assemblages to environmental change during the early Late-glacial at Gerzensee, Switzerland. *Palaeogeography, Palaeoclimatology, Palaeoecology* **391**: 90–98.

Brooks SJ, Langdon PG. 2014. Summer temperature gradients in northwest Europe during the Lateglacial to early Holocene transition (15–8 ka BP) inferred from chironomid assemblages. *Quaternary International* **341**: 80–90.

Brooks SJ, Langdon PG, Heiri O. 2007. The identification and use of Palaearctic Chironomidae larvae in palaeoecology. Quaternary Research Association.

Brooks SJ, Axford Y, Heiri O, Langdon PG, Larocque-Tobler I. 2012. Chironomids can be reliable proxies for Holocene temperatures. A comment on Velle *et al*.(2010). *The Holocene* **22**(12): 1495–1500.

Brooks SJ, Davies KL, Mather KA, Matthews IP, Lowe JJ. 2016. Chironomid-inferred summer temperatures for the Last Glacial–Interglacial Transition from a lake sediment sequence in Muir Park Reservoir, west-central Scotland. *Journal of Quaternary Science* **31**(3): 214–224.

Bunting MJ. 1994. Vegetation history of Orkney, Scotland: Pollen records from two small basins in west Mainland. *New Phytologist* **128**(4): 771–792.

Burjachs F, Jones SE, Giralt S, de Pablo JFL. 2016. Lateglacial to Early Holocene recursive aridity events in the SE Mediterranean Iberian Peninsula: The Salines playa lake case study. *Quaternary International* **403**: 187–200.

Candy I, Stephens M, Hancock J, Waghorne R. 2011. Palaeoenvironments of ancient humans in Britain: the application of oxygen and carbon isotopes to the reconstruction of Pleistocene environments. In *The Ancient Human Occupation of Britain*, Ashton N, Lewis SG, Stringer C (eds). Elsevier: London; 23–38.

Candy I, Farry A, Darvill CM, Palmer A, Blockley SPE, Matthews IP, MacLeod A, Deeprose L, Farley N, Kearney R, Conneller C. 2015. The evolution of Palaeolake Flixton and the environmental context of Star Carr: an oxygen and carbon isotopic record of environmental change for the early Holocene. *Proceedings of the Geologists' Association* **126**(1): 60–71.

Candy I, Abrook A, Elliot F, Lincoln PC, Matthews IP, Palmer AP. 2016. Oxygen Isotope evidence for high magnitude, abrupt climatic events during the Late-Glacial Interstadial in northwest Europe: Analysis of a lacustrine sequence from the site of Tirinie, Scottish Highlands. *Journal of Quaternary Science* **31**(6): 607–621.

Clark CD, Hughes AL, Greenwood SL, Jordan C, Sejrup HP. 2012. Pattern and timing of retreat of the last British-Irish Ice Sheet. *Quaternary Science Reviews* **44**: 112–146.

Clark PU, Marshall SJ, Clarke GK, Hostetler SW, Licciardi JM, Teller JT. 2001. Freshwater forcing of abrupt climate change during the last glaciation. *Science* **293**(5528): 283–287.

Clark PU, Pisias NG, Stocker TF, Weaver AJ. 2002. The role of the thermohaline circulation in abrupt climate change. *Nature* **415**(6874): 863–869.

Clegg BF, Kelly R, Clarke GH, Walker IR, Hu FS. 2011. Nonlinear response of summer temperature to Holocene insolation forcing in Alaska. *Proceedings of the National Academy of Sciences* **108**(48): 19299–19304.

Cochrane AA. 2020. Palaeoclimate reconstruction of the Northern Isles of Scotland, and Caithness, during the Last Glacial – Interglacial Transition. Unpublished PhD thesis, University of Stirling pp. 358

Cole GA, Weihe PE. 2015. Textbook of limnology. Waveland Press.

Coope GR, Pennington WP. 1977. The Windermere Interstadial of the Late Devensian. *Philosophical Transactions of the Royal Society. London* **B280**: 337–39.

Coope GR, Lemdahl G, Lowe JJ, Walkling A. 1998. Temperature gradients in northern Europe during the last glacial–Holocene transition (14-9 14C kyr BP) interpreted from coleopteran assemblages. *Journal of Quaternary Science* **13**(5): 419–433.

Dahl SO, Nesje A, Lie Ø, Fjordheim K, Matthews JA. 2002. Timing, equilibrium-line altitudes and climatic implications of two early-Holocene glacier readvances during the Erdalen Event at Jostedalsbreen, western Norway. *The Holocene* **12**(1): 17–25.

Dansgaard W, Johnsen SJ, Clausen HB, Dahl-Jensen D, Gundestrup NS, Hammer CU, Hvidberg CS, Steffensen JP, Sveinbjörnsdottir AE, Jouzel J, Bond G. 1993. Evidence for general instability of past climate from a 250-kyr ice-core record. *Nature* **364**(6434): 218–220.

Davies SM, Abbott PM, Pearce NJ, Wastegård S, Blockley SP. 2012. Integrating the INTIMATE records using tephrochronology: rising to the challenge. *Quaternary Science Reviews* **36**: 11–27.

De'ath G. 1999. Principal curves: a new technique for indirect and direct gradient analysis. *Ecology* **80**: 2237–2253.

Denton GH, Alley RB, Comer GC, Broecker WS. 2005. The role of seasonality in abrupt climate change. *Quaternary Science Reviews* **24**(10-11): 1159–1182.

Diefendorf AF, Patterson WP, Mullins HT, Tibert N, Martini A. 2006. Evidence for high-frequency late Glacial to mid-Holocene (16,800 to 5500 cal yr BP) climate variability from oxygen isotope values of Lough Inchiquin, Ireland. *Quaternary Research* **65**(1): 78–86.

Fiłoc M, Kupryjanowicz M, Rzodkiewicz M, Suchora M. 2018. Response of terrestrial and lake environments in NE Poland to Preboreal cold oscillations (PBO). *Quaternary International* 101–117.

Farrell M, Bunting MJ, Lee DH, Thomas A. 2014. Neolithic settlement at the woodland's edge: palynological data and timber architecture in Orkney, Scotland. *Journal of archaeological science* **51**: 225–236.

Fisher TG, Smith DG, Andrews JT. 2002. Preboreal oscillation caused by a glacial Lake Agassiz flood. *Quaternary Science Reviews* **21**(8-9): 873–878.

Grimm EC. 1987. CONISS: A FORTRAN 77 program for graphically constrained cluster analysis by the method of incremental sum of squares. *Computers & Geosciences* **3**: 13–35.

Hall AM, Riding JB, Brown JF. 2016. The last glaciation in Orkney, Scotland: glacial stratigraphy, event sequence and flow paths. *Scottish Journal of Geology* **52**(2): 90–101.

Hastie T, Stuetzle W. 1989. Principal curves. *Journal of the American Statistical Association* **84**: 502–516.

Heiri O, Lotter AF. 2001. Effect of low count sums on quantitative environmental reconstructions: an example using subfossil chironomids. *Journal of Paleolimnology* **26**(3): 343–350.

Heiri O, Lotter AF, Hausmann S, Kienast F. 2003. A chironomid- based Holocene summer air temperature reconstruction from the Swiss Alps. *The Holocene* **13**: 477–484.

Heiri O, Brooks SJ, Birks HJB, Lotter AF. 2011. A 274-lake calibration data-set and inference model for chironomid-based summer air temperature reconstruction in Europe. *Quaternary Science Reviews* **30**(23-24): 3445–3456.

Heiri O, Brooks SJ, Renssen H, Bedford A, Hazekamp M, Ilyashuk B, Jeffers ES, Lang B, Kirilova E, Kuiper S, Millet L. 2014. Validation of climate model-inferred regional temperature change for late-glacial Europe. *Nature communications* **5**: 1–7.

Holmes JA, Tindall J, Roberts N, Marshall W, Marshall JD, Bingham A, Feeser I, O'Connell M, Atkinson T, Jourdan AL, March A. 2016. Lake isotope records of the 8200-year cooling event in western Ireland: Comparison with model simulations. *Quaternary Science Reviews* **131**: 341–349.

Isarin RF, Bohncke SJ. 1999. Mean July temperatures during the Younger Dryas in northwestern and central Europe as inferred from climate indicator plant species. *Quaternary Research* **51**(2): 158–173.

Jennings A, Thordarson T, Zalzal K, Stoner J, Hayward C, Geirsdóttir Á, Miller G. 2014. Holocene tephra from Iceland and Alaska in SE Greenland shelf sediments. *Geological Society, London, Special Publications* **398**(1): 157–193.

Jessen CA, Rundgren M, Björck S, Andresen CS, Conley DJ. 2008. Variability and seasonality of North Atlantic climate during the early Holocene: evidence from Faroe Island lake sediments. *The Holocene* **18**: 851–860.

Johnsen SJ, Clausen HB, Dansgaard W, Fuhrer K, Gundestrup N, Hammer CU, Iversen P, Jouzel J, Stauffer B. 1992. Irregular glacial interstadials recorded in a new Greenland ice core. *Nature* **359**(6393): 311–313.

Jones VJ, Solovieva N, Self AE, McGowan S, Rosén P, Salonen JS, Seppä H, Väliranta M, Parrott E, Brooks SJ. 2011. The influence of Holocene tree-line advance and retreat on an arctic lake ecosystem: a multi-proxy study from Kharinei Lake, North Eastern European Russia. *Journal of Paleolimnology* **46**(1): 123–137.

Karpuz NK, Jansen E. 1992. A high-resolution diatom record of the last deglaciation from the SE Norwegian Sea: Documentation of rapid climatic changes. *Paleoceanography* **7**(4): 499–520.

Kaufman D, McKay N, Routson C *et al*. 2020. A global database of Holocene paleotemperature records. *Scientific Data* **7**(1): 1–34.

Kearney R, Albert PG, Staff RA, Pál I, Veres D, Magyari E, Ramsey CB. 2018. Ultra-distal fine ash occurrences of the Icelandic Askja-S Plinian eruption deposits in Southern Carpathian lakes: New age constraints on a continental scale tephrostratigraphic marker. *Quaternary Science Reviews* **188**: 174–182.

Kelts K, Hsü KJ. 1978. Freshwater carbonate sedimentation. In *Lakes: Chemistry, Geology, Physics*, Lerman A (ed). Springer: New York; 295–323.

Lang B, Bedford A, Brooks SJ, Jones RT, Richardson N, Birks HJB, Marshall JD. 2010. Early-Holocene temperature variability inferred from chironomid assemblages at Hawes. *Water, northwest England. The Holocene* **20**(6): 943–954.

Larocque-Tobler I, Heiri O, Wehrli M. 2010. Late Glacial and Holocene temperature changes at Egelsee, Switzerland, reconstructed using subfossil chironomids. *Journal of Paleolimnology* **43**(4): 649–666.

Leng MJ, Marshall JD. 2004. Palaeoclimate interpretation of stable isotope data from lake sediment archives. *Quaternary Science Reviews* **23**(7): 811–831.

Lind EM, Wastegård S, Larsen JJ. 2013. A Late Younger Dryas-Early Holocene tephrostratigraphy for Fosen, Central Norway. *Journal of Quaternary Science* **28**(8): 803–811.

Longva O, Thoresen MK. 1991. Iceberg scours, iceberg gravity craters and current erosion marks from a gigantic Preboreal flood in southeastern Norway. *Boreas* **20**(1): 47–62.

Lowe JJ, Walker MJ. 2000. Radiocarbon Dating the Last Glacial-Interglacial Transition (Ca. 14–9 ^{14}C Ka BP) in Terrestrial and Marine Records: The Need for New Quality Assurance Protocols. *Radiocarbon* **42**(1): 53–68.

Lowe JJ, Rasmussen SO, Björck S, Hoek WZ, Steffensen JP, Walker MJ, Yu ZC. 2008. Synchronisation of palaeoenvironmental events in the North Atlantic region during the Last Termination: a revised protocol recommended by the INTIMATE group. *Quaternary Science Reviews* **27**(1): 6–17.

Lowe J, Matthews I, Mayfield R, Lincoln P, Palmer A, Staff R, Timms R. 2019. On the timing of retreat of the Loch Lomond ('Younger Dryas') Readvance icefield in the SW Scottish Highlands and its wider significance. *Quaternary Science Reviews* **219**: 171–186.

Mangili C, Brauer A, Plessen B, Dulski P, Moscariello A, Naumann R. 2010. 'Effects of detrital carbonate on stable oxygen and carbon isotope data from varved sediments of the interglacial Pianico palaeolake (Southern Alps, Italy). *Journal of Quaternary Science* **25**(2): 135–145.

Marshall JD, Jones RT, Crowley SF, Oldfield F, Nash S, Bedford A. 2002. A high resolution late-glacial isotopic record from Hawes Water, northwest England: Climatic oscillations: Calibration and comparison of palaeotemperature proxies. *Palaeogeography, Palaeoclimatology, Palaeoecology* **185**(1): 25–40.

Marshall JD, Lang B, Crowley SF, Weedon GP, van Calsteren P, Fisher EH, Holme R, Holmes JA, Jones RT, Bedford A, Brooks SJ. 2007. Terrestrial impact of abrupt changes in the North Atlantic thermohaline circulation: Early Holocene, UK. *Geology* **35**(7): 639–642.

Matthews IP, Birks HH, Bourne AJ, Brooks SJ, Lowe JJ, MacLeod A, Pyne-O'Donnell SDF. 2011. New age estimates and climatostratigraphic correlations for the Borrobol and Penifiler Tephras: evidence from Abernethy Forest, Scotland. *Journal of Quaternary Science* **26**(3): 247–252.

Matthews JA, Shakesby RA, Schnabel C, Freeman S. 2008. Cosmogenic ^{10}Be and ^{26}Al ages of Holocene moraines in southern Norway I: testing the method and confirmation of the date of the Erdalen Event (*c.* 10 ka) at its type-site. *The Holocene* **18**(8): 1155–1164.

Mekhaldi F, Czymzik M, Adolphi F, Sjolte J, Björck S, Aldahan A, Brauer A, Martín-Puertas C, Possnert G, Muscheler R. 2019. Radionuclide wiggle-matching reveals a non-synchronous Early Holocene climate oscillation in Greenland and Western Europe around a grand solar minimum. *Climate of the Past Discussions* 1–23.

Met Office. 2020. UK Climate averages, Kirkwall. https://www.metoffice.gov.uk/research/climate/maps-and-data/uk-climate-averages/gfmzqh0rc [last accessed on 01/07/2020].

Moar NT. 1969. Two pollen diagrams from the Mainland, Orkney Islands. *New Phytologist* **68**(1): 201–208.

Moller Pillot H, Klink A. 2003. Chironomidae larvae: Key to higher taxa and species of the lowlands of Northwestern Europe, Expert Center for Taxonomic Identification (ETI), University of Amsterdam.

Moreno A, Svensson A, Brooks SJ, Connor S, Engels S, Fletcher W, Genty D, Heiri O, Labuhn I, Perşoiu A, Peyron O, Sedori L, Valero-Garcés B, Wulf S, Zanchetta G. 2014. A compilation of Western European terrestrial records 60–8 ka BP: towards an understanding of latitudinal climatic gradients. *Quaternary Science Reviews* **106**: 167–185.

Muscheler R, Beer J, Wagner G, Laj C, Kissel C, Raisbeck GM, Yiou F, Kubik PW. 2004. Changes in the carbon cycle during the last deglaciation as indicated by the comparison of 10Be and 14C records. *Earth and Planetary Science Letters* **219**(3-4): 325–340.

Mykura W, Flinn D, May F. 1976. British regional geology: Orkney and Shetland.

Nesje A, Kvamme M, Rye N, Løvlie R. 1991. Holocene glacial and climate history of the Jostedalsbreen region, western Norway; evidence from lake sediments and terrestrial deposits. *Quaternary Science Reviews* **10**(1): 87–114.

Nesje A, Dahl SO. 1991. Late Holocene glacier fluctuations in Bevringsdalen, Jostedalsbreen region, western Norway (ca 3200-1400 BP). *The Holocene* **1**(1): 1–7.

Nesje A, Dahl SO, Bakke J. 2004. Were abrupt Lateglacial and early-Holocene climatic changes in northwest Europe linked to freshwater outbursts to the North Atlantic and Arctic Oceans? *The Holocene* **14**(2): 299–310.

Nesje A, Bakke J, Brooks SJ, Kaufman DS, Kihlberg E, Trachsel M, D'Andrea WJ, Matthews JA. 2014. Late glacial and Holocene

environmental changes inferred from sediments in Lake Myklevatnet, Nordfjord, western Norway. *Vegetation history and archaeobotany* **23**(3): 229–248.

Oksanen J, Blanchet FG, Friendly M, Kindt R, Legendre P, McGlinn D, Minchin PR, O'Hara RB, Simpson GL, Solymos P, Stevens HH, Szoecs E, Wagner H. (2017). Package 'vegan': community ecology package, version:2.4-4.

Óladóttir BA, Thordarson T, Geirsdóttir Á, Jóhannsdóttir GE, Mangerud J. 2020. The Saksunarvatn Ash and the G10ka series tephra. Review and current state of knowledge. *Quaternary Geochronology* **56** 101041.

Palmer S, Walker I, Heinrichs M, Scudder G. 2002. Postglacial midge community change and Holocene palaeotemperature reconstructions near treeline, southern British Columbia (Canada). *Journal of Paleolimnology* **28**(4): 469–490.

Phillips WM, Hall AM, Ballantyne CK, Binnie S, Kubik PW, Freeman S. 2008. Extent of the last ice sheet in northern Scotland tested with cosmogenic ^{10}Be exposure ages. *Journal of Quaternary Science* **23**(2): 101–107.

Płóciennik M, Self A, Birks HJB, Brooks SJ. 2011. Chironomidae (Insecta: Diptera) succession in Żabieniec bog and its palaeo-lake (central Poland) through the Late Weichselian and Holocene. *Palaeogeography, Palaeoclimatology, Palaeoecology* **307**(1-4): 150–167.

Rae DA. 1976. Aspects of Glaciation in Orkney. Unpublished PhD Thesis, University of Liverpool pp. 469.

Ranner PH, Allen JR, Huntley B. 2005. A new early Holocene cryptotephra from northwest Scotland. *Journal of Quaternary Science* **20**(3): 201–208.

Rasmussen SO, Vinther BM, Clausen HB, Andersen KK. 2007. Early Holocene climate oscillations recorded in three Greenland ice cores. *Quaternary Science Reviews* **26**(15): 1907–1914.

Rasmussen SO, Bigler M, Blockley SP, Blunier T, Buchardt SL, Clausen HB, Cvijanovic I, Dahl-Jensen D, Johnsen SJ, Fischer H, Gkinis V, Guillevic M, Hoek WZ, Lowe JJ, Pedro JB, Popp T, Seierstad IK, Steffensen JP, Svensson AM, Vallelonga P, Vinther BM, Walker MJC, Wheatley JJ, Winsrtup M. 2014. A stratigraphic framework for abrupt climatic changes during the Last Glacial period based on three synchronized Greenland ice-core records: refining and extending the INTIMATE event stratigraphy. *Quaternary Science Reviews* **106**: 14–28.

Reimer PJ, Austin WEN, Bard E, Bayliss A, Blackwell PG, Bronk Ramsey C, Butzin M, Cheng H, Edwards RL, Friedrich M, Grootes PM, Guilderson TP, Hajdas I, Heaton TJ, Hogg AG, Hughen KA, Kromer B, Manning SW, Muscheler R, Palmer JG, Pearson C, van der Plicht J, Reimer RW, Richards DA, Scott EM, Southon JR, Turney CSM, Wacker L, Adolphi F, Büntgen U, Capano M, Fahrni SM, Fogtmann-Schulz A, Friedrich R, Köhler P, Kudsk S, Miyake F, Olsen J, Reinig F, Sakamoto M, Sookdeo A, Talamo S. 2020. The IntCal20 Northern Hemisphere Radiocarbon Age Calibration Curve (0–55 cal kBP). *Radiocarbon* **62**(4): 725–757.

Rose J. 1985. The Dimlington Stadial/Dimlington Chronozone: a proposal for naming the main glacial episode of the Late Devensian in Britain. *Boreas* **14**(3): 225–230.

Rozanski K, Araguas-Araguas L, Gonfiantini R. 1992. Relation between long-term trends of oxygen-18 isotope composition of precipitation and climate. *Science* **258**(5084): 981–985.

Ruddiman WF, Raymo M, Martinson DG, Clement BM, Backman J. 1989. Pleistocene evolution: northern hemisphere ice sheets and North Atlantic Ocean. *Paleoceanography* **4**(4): 353–412.

Samartin S, Heiri O, Vescovi E, Brooks SJ, Tinner W. 2012. Lateglacial and early Holocene summer temperatures in the southern Swiss Alps reconstructed using fossil chironomids. *Journal of Quaternary Science* **27**(3): 279–289.

Shakesby RA, Matthews JA, Winkler S, Fabel D, Dresser PQ. 2020. Early-Holocene moraine chronology, Sognefjell area, southern Norway: evidence for multiple glacial and climatic fluctuations within the Erdalen Event (~10.2–9.7 ka). *Norwegian Journal of Geology* **100** 202014.

Shala S, Helmens KF, Luoto TP, Salonen JS, Väliranta M, Weckström J. 2017. Comparison of quantitative Holocene temperature reconstructions using multiple proxies from a northern boreal lake. *The Holocene* **27**(11): 1745–1755.

Simpson G. 2020. Analogue: Analogue and Weighted Averaging Methods for Palaeoecology. R package version (0.17-4).

Simpson GL, Birks HJB. 2012. Statistical learning in Palaeolimnology. In *Tracking Environmental Change Using Lake Sediments. Volume 5: Data Handling and Numerical Techniques*, Birks HJB, Lotter AF, Juggins S, Smol JP (eds). Kluwer Academic Publishers: Dordrecht, The Netherlands; 249–327.

Smith DE, Harrison S, Firth CR, Jordan JT. 2011. The early Holocene sea level rise. *Quaternary Science Reviews* **30**(15-16): 1846–1860.

Steffensen JP, Andersen KK, Bigler M, Clausen HB, Dahl-Jensen D, Fischer H, Goto-Azuma K, Hansson M, Johnsen SJ, Jouzel J, Masson-Delmotte V. 2008. 'High-resolution Greenland ice core data show abrupt climate change happens in few years. *Science* **321**(5889): 680–684.

Talbot MR. 1990. A review of the palaeohydrological interpretation of carbon and oxygen isotopic ratios in primary lacustrine carbonates. *Chemical Geology: Isotope Geoscience Section* **80**(4): 261–279.

Telford R. (2014a). Beyond nearest analogue distance. [Blog] Musings on Quantitative Palaeoecology. https://quantpalaeo.wordpress.com/2014/05/17/beyond-nearest-analogue-distance/ [Accessed June 2020].

Telford R. (2014b). Analogue quality, reconstruction quality. [Blog] Musings on Quantitative Palaeoecology. https://quantpalaeo.wordpress.com/2014/05/11/analogue-quality-reconstruction-quality/ [Accessed June 2020].

Teller JT, Leverington DW, Mann JD. 2002. Freshwater outbursts to the oceans from glacial Lake Agassiz and their role in climate change during the last deglaciation. *Quaternary Science Reviews* **21**(8-9): 879–887.

Timms R. 2016. Developing a refined tephrostratigraphy for Scotland, and constraining abrupt climatic oscillations of the Last Glacial-Interglacial Transition (ca 16-8 ka bp) using high resolution tephrochronologies. Unpublished PhD Thesis, Royal Holloway, University of London pp. 494.

Timms RGO, Matthews IP, Palmer AP, Candy I, Abel L. 2017. A high-resolution tephrostratigraphy from Quoyloo Meadow, Orkney, Scotland: Implications for the tephrostratigraphy of NW Europe during the Last Glacial-Interglacial Transition. *Quaternary Geochronology* **40**: 67–81.

Timms RGO, Matthews IP, Palmer AP, Candy I. 2018. Toward a tephrostratigraphic framework for the British Isles: A Last Glacial to Interglacial Transition (LGIT *c.* 16-8 ka) case study from Crudale Meadow, Orkney. *Quaternary Geochronology* **46**: 28–44.

Timms RGO, Matthews IP, Lowe JJ, Palmer AP, Weston DJ, MacLeod A, Blockley SP. 2019. Establishing tephrostratigraphic frameworks to aid the study of abrupt climatic and glacial transitions: a case study of the Last Glacial-Interglacial Transition in the British Isles (*c.* 16-8 ka BP). *Earth-Science Reviews* **192**: 34–64.

Tóth M, Magyari EK, Buczkó K, Braun M, Panagiotopoulos K, Heiri O. 2015. Chironomid-inferred Holocene temperature changes in the South Carpathians (Romania). *The Holocene* **25**(4): 569–582.

Troels-Smith J. 1955. Characterisation of unconsolidated sediments. *Danmarks Geologiske Undersoegelse* **4**: 1–73.

Tye GJ, Sherriff J, Candy I, Coxon P, Palmer A, McClymont EL, Schreve DC. 2016. The δ18O stratigraphy of the Hoxnian lacustrine sequence at Marks Tey, Essex, UK: implications for the climatic structure of MIS 11 in Britain. *Journal of Quaternary Science* **31**(2): 75–92.

Ullman DJ, Carlson AE, Hostetler SW, Clark PU, Cuzzone J, Milne GA, Winsor K, Caffee M. 2016. Final Laurentide ice-sheet deglaciation and Holocene climate-sea level change. *Quaternary Science Reviews* **152**: 49–59.

van Asch N, Hoek WZ. 2012. The impact of summer temperature changes on vegetation development in Ireland during the Weichselian Lateglacial Interstadial. *Journal of Quaternary Science* **27**(5): 441–450.

van der Plicht J, Van Geel B, Bohncke SJP, Bos JAA, Blaauw M, Speranza AOM, Muscheler R, Björck S. 2004. The Preboreal climate reversal and a subsequent solar-forced climate shift. *Journal of Quaternary Science* **19**(3): 263–269.

Velle G, Brooks SJ, Birks HJB, Willassen E. 2005. Chironomids as a tool for inferring Holocene climate: an assessment based on six sites in southern Scandinavia. *Quaternary Science Reviews* **24**(12-13): 1429–1462.

Vinther BM, Clausen HB, Johnsen SJ, Rasmussen SO, Andersen KK, Buchardt SL, Dahl-Jensen D, Seierstad IK, Siggaard-Andersen ML, Steffensen JP, Svensson A. 2006. A synchronized dating of three Greenland ice cores throughout the Holocene'. *Journal of Geophysical Research: Atmospheres* **111**(D13).

von Grafenstein U, Belmecheri S, Eicher U, van Raden J, Andersen N, Ammann B. 2013. The oxygen and carbon isotopic signatures of biogenic carbonates in Gerzensee, Switzerland, during the rapid warming around 14,685 years BP and the following interstadial. *Palaeogeography, Palaeoclimatology, Palaeoecology* **391**: 25–32.

Walker MJC, Bohncke SJP, Coope GR, O'Connell M, Usinger H, Verbruggen C. 1994. The Devensian/Weichselian Late-glacial in northwest Europe (Ireland, Britain, north Belgium, The Netherlands, northwest Germany). *Journal of Quaternary Science* **9**: 109–118.

Walker M, Lowe J. 2019. Lateglacial environmental change in Scotland. *Earth and Environmental Science Transactions of the Royal Society of Edinburgh* **110**(1-2): 173–198.

Walker M, Head MJ, Lowe J, Berkelhammer M, Björck S, Cheng H, Cwynar LC, Fisher D, Gkinis V, Long A, Newnham R, Rasmussen SO, Weiss H. 2019. Subdividing the Holocene Series/Epoch: formalization of stages/ages and subseries/subepochs, and designation of GSSPs and auxiliary stratotypes. *Journal of Quaternary Science* **34**: 173–186.

Wastegård S, Gudmundsdóttir ER, Lind EM, Timms RG, Björck S, Hannon GE, Olsen J, Rundgren M. 2018. Towards a Holocene tephrochronology for the Faroe Islands, North Atlantic. *Quaternary Science Reviews* **195**: 195–214.

Watson JE, Brooks SJ, Whitehouse NJ, Reimer PJ, Birks HJB, Turney CSM. 2010. Chironomid-inferred late-glacial summer air temperatures from Lough Nadourcan, Co. Donegal, Ireland. *Journal of Quaternary Science* **25**(8): 1200–1210.

Whittington G, Fallick AE, Edwards KJ. 1996. Stable oxygen isotope and pollen records from eastern Scotland and a consideration of Late-glacial and early Holocene climate change for Europe. *Journal of Quaternary Science* **11**(4): 327–340.

Whittington G, Edwards KJ, Zanchetta G, Keen DH, Bunting MJ, Fallick AE, Bryant CL. 2015. Lateglacial and early Holocene climates of the Atlantic margins of Europe: Stable isotope, mollusc and pollen records from Orkney, Scotland. *Quaternary Science Reviews* **122**: 112–130.

Wiederholm T. 1983. Chironomidae of the Holarctic region. Keys and diagnoses. Part I. Larvae. *Entomologica Scandynavica* **Supplement 1**: 1–457.

Wohlfarth B, Muschitiello F, L. Greenwood S, Andersson A, Kylander M, Smittenberg RH, Steinthorsdottir M, Watson J, Whitehouse NJ. 2017. Hässeldala–a key site for Last Termination climate events in northern Europe. *Boreas* **46**(2): 143–161.